Master of Science Thesis

Coupled Finite Element Simulation of Electrostrictive Fluids

by

Venkatesh Gopinath

Thesis submitted to the Swansea University in candidature for the degree of Master of Science

Supervisors: Dr. Antonio J Gil and Dr. Paul D Ledger

Civil and Computational Engineering Centre
College of Engineering
Swansea University, Swansea
United Kingdom

June 2011

DECLARATION

This work has not previously been accepted in substance for any degree and is not being currently submitted in candidature for any degree.

Signed.....(candidate)
Date.....

STATEMENT 1

This thesis is the result of my own investigation, except where otherwise stated. Other sources are acknowledged by footnotes giving explicit references. A bibliography is appended.

Signed.....(candidate)
Date.....

STATEMENT 2

I hereby give consent for my thesis, if accepted, to be available for photocopying and for inter-library loan, and for the title and summary to be made available to outside organizations.

Signed.....(candidate)
Date.....

Summary

The study investigates the coupled problem of electrostrictive fluids. A hp finite element method is used for the numerical analysis. Initially the individual fields of electrostatics and fluids are analysed. Firstly the benchmarking simulations for the electrostatics field are done and exponential convergence for the solutions is obtained. Next the fluid field is analysed. Initially the Navier-Stokes equations are simplified using appropriate assumptions to obtain Stokes flow equations. Afterwards, an equivalence between the Stokes flow equation and the linear elasticity equation is established for the limiting case of Poisson's ratio $\nu \to 0.5$. The penalty function formulation and the mixed approach for penalty formulation are used to obtain solution for the Stokes flow problem. Again the hp discretization is used and exponential convergence for all the benchmark problems is obtained.

After benchmarking the solvers for electrostatics and the fluid field, the coupled problem is analysed. Initially the governing equations for both the fluid and electrostatics fields are written. Next, the coupling mechanism involved in the case of electrostrictive fluid is elucidated clearly. Briefly, it can be described as follows. When the electrostatics field is analysed, the unknown potentials ϕ are obtained. Using the ϕ, the electric field is computed. This electric field induces a stress known as the electrostrictive stress, which then acts as a source term in the fluid problem. The coupled problem thus uses a staggered scheme for the coupled solution, since it is a one-way coupling. Furthermore, benchmarking simulations are carried out and exponential convergence for the solutions is obtained. As a novel exercise, a coupled problem is created and solved. Findings from this result are elaborated and current applications of this work are described.

Acknowledgements

I would like to express my heartfelt gratitude to my thesis supervisors, Dr. Paul D Ledger and Dr. Antonio J Gil. Right from the beginning of the thesis, they have been extremely helpful and patient. Apart from the technical knowledge they have imparted to me, they have also shown how a research project must be pursued. Their guidance throughout the thesis is invaluable to me. I would also take this opportunity to thank all my teachers at Swansea University and at International Center for Numerical Methods in Engineering (CIMNE), UPC Barcelona, for their help and guidance during the course work. Furthermore, I would like to thank my parents and my sister, for all their encouragements and support. A special thanks to my mother, without whose love, I would not be where I am. I would also like to thank all my friends in the Erasmus Mundus master studies, as well as colleagues and friends at Swansea and Barcelona for making my stay a pleasant one. Finally, I would like to show my gratitude to the European Commission for giving this great opportunity to study at such a technically world class place.

Contents

List of Figures

Chapter 1

Introduction

1.1 Introduction

Coupled problems in applied mechanics are generally defined as those requiring the solution of more than one physical process in order to represent the overall system adequately [4]. So, it is important to have an understanding of each of the physics involved. In this thesis a coupled analysis of a electrostrictive fluid is done. An electrostrictive fluid is a dielectric fluid which deforms under the application of an electric field. A simplification is used in this thesis for solving fluid flows where the Stokes flow is used instead of full system of Navier Stokes equations. And the electromagnetic behavior is also simplified by restricting consideration to electrostatics. Even with such simplification, the work in this thesis can be directly applied to to applications such as the CPU cooling liquids and micro motors, electroosmotic flows etc.

Some of the examples of electrostrictive fluids are described as follows. In the micro motor application [5] the Electro-Conjugate Fluids (ECF) are used. What actually happens here is that, the dielectric fluid moves to a region of higher energy-density countering normal fluid movement from high to low pressure. An example of such motor is shown in Figure 1.1.

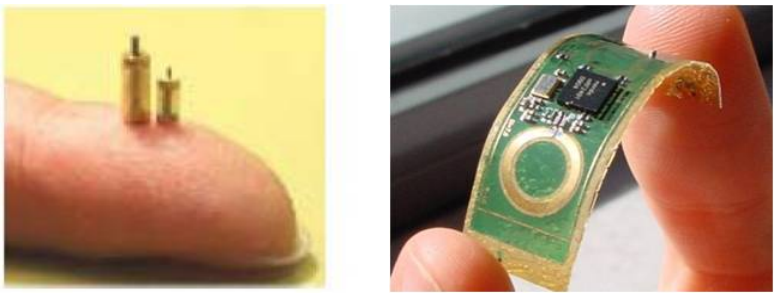

Figure 1.1: Micro motor which uses electro-conjugate fluids and a flexible electronic chip

Another example would be in the case of electro-rheological fluid application in the case of flexible electronics. Here the fluid viscosity is a function of the electric field. When Electric field is applied to the fluid, its viscosity goes up rapidly and it tends to behave almost like a solid. Such phenomena are also used in making body armors for combat forces. An example of a flexible electronic chip is shown in Figure. 1.1. More recently the company Kronos air technology [6] are researching on electrostrictive fluid accelerators for a method of controlling fluid flows for commercially useful airflow rates. Potential applications include air purifiers, CPU coolers, electro-acoustics etc.

Another important application is in the fluid mixing problem in laminar flow systems. In microfluidic systems, diffusion is often negligible compared to advection in the flow. Conventional methods, applied to create mixing in macro-scale fows, require sufficiently large Reynolds numbers, and become ineffective when applied to micro-scale flows [7]. As a consequence, alternative techniques to enhance mixing efficiency in small systems are required. This is done using the phenomenon of electroosmotic flows, which is a direct application of the work done in the project along with some minor extensions. An example of the recent research work done at Technical University of Darmstadt [1] is shown in Figure. 1.2.

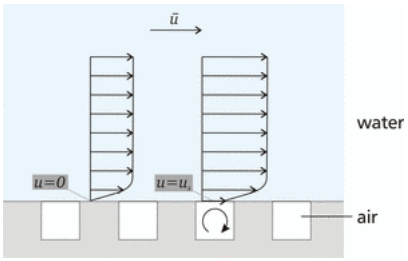

Figure 1.2: Electroosmotic flow over super-hydrophobic surface [1]

It is a flow over a super-hydrophobic surface which has both no-slip walls and slipping walls. The flow is under the influence of an electric field. In micro channel flows, such a surface could be effective as reduce the effect of the no-slip walls, which impede the flow. However, simulations are required to know exactly how far the electric field helps to obtain optimal fluid flow in these channels and it remains an open question in this case.

Experimental investigation of such phenomena are very expensive and is not possible in some cases, so a numerical solution for such problems are an effective alternative to analyse such phenomena. Due to the above mentioned applications, motivation for solving such challenging problems drives the work done in the thesis.

The key steps to be identified for a coupled simulation are defined as follows

1. Physical problem to be analysed.
2. Understand the physics involved and what the coupling mechanisms are.
3. Be able to accurately predict each of the physics independently.
4. Formulate a procedure which takes full account of all coupling mechanisms involved.

Furthermore, coupled systems fall into two categories [8]. The first case is where the coupling occurs on domain interfaces, i.e. via the boundary conditions imposed at the interfaces. The second case is where the domains of the individual problems overlap and the coupling occurs through the governing differential equations describing different physical phenomena. In this thesis the coupled problem comes under second case. Furthermore, coupling in a problem can be strong or weak. A strong

coupling is where each subsystem causes a response in all other subsystems. A weak coupling may involve the effect of one subsystem on another but not viceversa.

1.2 Numerical technique - *hp* finite element method

The above discussion involved the challenging problems in physics which are not easy to recreate as an experiment. Moreover, modeling of such phenomena is difficult since these mechanisms are highly non-linear in nature and most of the cases do not have an analytical solution. Hence a numerical method is required to accurately predict the behavior of each of the physics involved in the coupled problem as well as the coupling mechanisms that exists between them. It is well established that the finite element method is a powerful method for the analysis of both electrostatics and fluid flow.

Usually lower order approximations are employed, but in the quest for higher levels of accuracy, higher order elements are used. Traditional higher order finite element methods have been discussed in the wide range of technical literature such as [9, 10]. Since technology has improved in the area of computer power, it is now become affordable that higher order solutions are routinely undertaken. In order to obtain highly accurate solutions, one must perform certain extensions or refinements of the finite element discretization. The refinement of the mesh spacing is called h refinement and the one based on increasing the polynomial degree of elements is called the p refinement and if we do both these refinements simultaneously, then it is called hp refinement. In the case of a smooth problem, p refinement alone is the best strategy as it results in exponential convergence of the solution. However in certain class of problems employing h refinement at certain regions of the domain, for example in the presence of a singularity in the domain, proves to be better. An optimal combination of h and p refinement is particularly useful to obtain a exponential convergence for wide variety of industrial problems which contain singularities as well as regions with smooth solutions. When both h and p are simultaneously refined, it is known as the hp finite element method.

1.2.1 Higher order shape functions in one dimension

In the higher order approximations, there are two different type of shape functions which can be employed. The first type is the nodal type of shape function. In the nodal type of shape functions, each level of approximation results in completely new shape functions, hence the equation set has to be entirely reevaluated [9]. The other approach is by the way of hierarchical shape functions. The name hierarchical results from the fact that successive higher order refinements are additive in nature. If hierarchical forms of shape functions are employed, then as the approximation is refined, new basis functions are added to the existing set and the matrices produced at the previous stage need not be recomputed. If the chosen functions are orthogonal(or close to) in their inner product, there is better conditioning of the resulting matrices. Furthermore the coupling between equations disappear if completely orthogonal trignometic trial functions and Galerkin method is used and the matrix forms a highly diagonal structure [9]. Most of the recently developed higher order formulations employ hierarchical forms due to their advantage in terms of the ease of efficient computing. The one dimensional shape functions are introduced below, in order to provide a clarity on the difference in the approaches to higher order shape functions.

In the nodal approach the degrees of freedom correspond to specific solution points. Using the Lagrange interpolation polynomial, the element shape functions for the linear, quadratic elements are stated as follows. In terms of the normalized local element coordinate ξ, which is defined within the range $-1 \leq \xi \leq 1$, the linear shape functions which is associated with the nodes $\xi = \pm 1$ are defined as

$$N_0 = -\frac{\xi - 1}{2}, \ \frac{dN_0}{d\xi} = \frac{1}{2} \tag{1.1}$$

$$N_1 = -\frac{\xi + 1}{2}, \ \frac{dN_1}{d\xi} = \frac{1}{2} \tag{1.2}$$

For the quadratic shape functions which are associated with the nodes at $\xi = \pm 1$

and $\xi = 0$, are

$$\begin{aligned} N_0 &= -\frac{\xi(\xi-1)}{2}, & \frac{dN_0}{d\xi} &= -\xi + \frac{1}{2} \\ N_1 &= -(\xi-1)(\xi+1), & \frac{dN_1}{d\xi} &= -2\xi \\ N_3 &= \frac{\xi(\xi+1)}{2}, & \frac{dN_2}{d\xi} &= \xi + \frac{1}{2} \end{aligned} \tag{1.3}$$

Now, if the the order is continually increased, then this approach could be able to obtain the cubic shape function and so on. Also, when the order is increased, improved results are obtainable with smaller number of total unknowns [9] as compared to lower order elements. However, this would require new set of associated nodes for each new order, which leads to completely new set of shape functions. This, in a context of a problem would lead to new definitions of the stiffness matrix for successive increase in the order of the elements. This would be a computationally expensive approach. Now, regarding the hierarchical shape function, the previous order of approximation is retained and a new function is added. Denoting this shape function as version 1, in terms of ξ it can be defined as

$$N_p = \alpha_0 + \alpha_1\xi + \alpha_2\xi^2 + ... + \alpha_p\xi^p \tag{1.4}$$

The linear shape functions are the same as defined before. However, to obtain the quadratic shape function, the additional shape function is needed as

$$N_2 = \alpha_0 + \alpha_1\xi + \alpha_2\xi^2 \tag{1.5}$$

which is such that $N_2 = 0$ at $\xi = \pm 1$. This leads to $\alpha_1 = 0$ and $\alpha_0 = -\alpha_2$. Choosing $N_2 = 1$ when $\xi = 0$, then the additional quadratic shape function can be written as

$$N_2 = 1 - \xi^2, \ \frac{dN_2}{d\xi} = -2\xi \tag{1.6}$$

Similarly the additional cubic shape functions can be obtained. Therefore, in terms of programmability, the hierarchical approach is better than the nodal approach for higher order shape functions. However, the above mentioned hierarchical shape function does not do well in terms of conditioning of the stiffness matrix as it is shown in

the appendix. In the derivation of hierarchical shape functions, there exists a freedom in choosing the co-efficient that corresponds to the new additional parameter [11]. So, one can derive new hierarchical shape functions which have better conditioning properties. An alternative description of the shapefunctions for $p \geq 2$ is given by

$$N_p(\xi) = \begin{cases} \frac{1}{p!}(\xi^p - 1) \\ \frac{1}{p!}(\xi^p - \xi) \end{cases}, \quad \frac{dN_p}{d\xi} \begin{cases} \frac{1}{p!}(p\xi^{p-1}) \\ \frac{1}{p!}(p\xi^{p-1} - 1) \end{cases} \tag{1.7}$$

where p$\geq$ 2 is the order of the polynomial. A further alternative is where the shape functions are defined as the integral of the Legendre polynomials. The Legendre polynomials are defined as

$$P_p(\xi) = \frac{1}{(p-1)!}\frac{1}{2^{p-1}}\frac{dP^p}{d\xi^p}[(\xi^2 - 1)^p] \tag{1.8}$$

and corresponding shape functions are

$$N_p(\xi) = \frac{1}{2p-1}\big(P_p(\xi) - P_{p-2}(\xi)\big), \ \frac{dN_p}{d\xi}(\xi) = \frac{1}{2p-1}\left(\frac{dP_p}{d\xi}(\xi) - \frac{dP_{p-1}}{d\xi}(\xi)\right) \tag{1.9}$$

As a *precursor* to the thesis, a finite element analysis using the above mentioned shape functions was done using an existing code which solves the Helmholtz equation in 1D. The MATLAB code in [11] was used for this purpose. Higher order shape functions are used and the difference between h refinement and p refinement are elaborated. The difference between nodal and hierarchical shape functions are noted from the results obtained. Also the effect of condition number is discussed in the context of h and p refinement. These results are described in the appendix.

1.2.2 Overview of the coupling mechanisms

There are different coupling mechanisms depending on whether the problem is strongly coupled or weakly coupled. Generally a solution procedure must be accurate, robust and computationally efficient. Some of the methods which can be used for solving a coupled problem, like the one described in the thesis, could be a block Gauss-Seidel method, where numerical implementation of coupling involves solving each problem

system separately in an iterative fashion such that any change in one system causes a response in the other system. Another way to resolve the coupled problem is by using the Newton-Rapshon method, where numerical implementation of this type involve solving both the systems which are coupled, simultaneously using a single block matrix.

1.3 Aim, overview and work to be done

1.3.1 Aim of the thesis

This thesis aims to to develop a coupled 2D finite element solver with *hp* discretization for the electrostrictive fluid. When the domains of electrostatics and fluid mechanics overlap in the coupled system, the variables on each domain have an interdependence. The electric field output from the electrostatics solver affects the stresses in the fluid mechanical system.

As such, the thesis can be split in to three tasks. Firstly the finite element analysis of the electrostatics problem, secondly the finite element analysis of the fluid mechanics problem and finally the coupled electrostrictive fluid problem. A *hp* finite element methodology will be employed for both the solution of the electrostatics and fluid flow problems. In particular, a penalty function formulation and mixed approach for the penalty formulation is utilized for solving the fluid problem and it is hoped that the *hp* discretization will overcome the problem of volumetric locking. The coupled solution will employ a staggered scheme where first, electrostatic fields are computed and subsequently the stresses induced by them are computed and they are used as a source term for the Stokes flow solution. An advanced starting point was provided through existing *hp* finite element solvers for both electrostatics and linear elasticity.

1.3.2 Overview of the thesis

The thesis is structured into five parts. The chapter 1 and chapter 5 deal with introduction and conclusions respectively, and chapters 2, 3 and 4 deal with the

work done in the thesis. The following description of the chapters lead to a general overview to the reader.

Chapter 1 In this chapter the need for coupled analysis is explained with some examples and significance of higher order finite element methods is elaborated, the results of which elucidates the the reasons for higher order versions of the finite elements.

Chapter 2 This chapter deals with the finite element formulation of the electrostatics problem. The benchmark numerical simulations for the same are performed, showing convergence for h and p refinement.

Chapter 3 In this chapter the finite element analysis of the fluid mechanics problem is performed. The particular problem chosen for the analysis is the Stokes flow. Its connection to the problem of linear elasticity is described in particular the penalty function method and the mixed method for penalty formulation are used for the simulations. The benchmark numerical simulations are performed for h and p refinement.

Chapter 4 In this chapter, the coupled phenomena of electrostatics field and fluid field are simulated. The boundary value problems of both the fields are written initially. Next the coupling mechanism is explained and the finite element formulation is shown. Following that, the algorithm implemented in the project is shown. Later the benchmark problem is explained. Next a numerical example is defined, which considers the coupling of the benchmark problems in electrostatics and fluid mechanics. Later the numerical results are shown for the benchmark problem along with the convergence analysis. Lastly the simulation results for the numerical exercise is shown along with some findings.

Chapter 5 This chapter deals with the conclusion and summary of the thesis. It also sheds light on further extension of the research.

1.3.3 Work to be done

The following tasks are to be done along the course of the thesis.

1 Perform benchmark numerical simulations for the electrostatics using the provided *hp* FEM code.

2 To extend the *hp* FEM code, in order to compute the electric field at each integration point and make a provision in the code for permittivity to be inputted as a tensor.

3 Perform benchmark numerical simulations for penalty function method and mixed approach for penalty formulation using the provided code.

4 To make arrangements in the code for inputting velocity boundary conditions for the Poiseiulle's flow at the higher order edges.

5 To input the source term for the benchmark problem and accordingly put the exact solutions where necessary.

6 Perform benchmark numerical simulations after doing the above mentioned modifications of the code provided. Also write generalized postprocessing scripts to extract data at any point for plotting velocity curves in order to benchmark the lid driven cavity problem.

7 To completely implement the one-way coupled solver for the electrostrictive fluid problem.

8 To benchmark the coupled solver with convergence plots.

9 To create and solve a numerical exercise.

Chapter 2

Analysis of the Electrostatics field

2.1 Introduction

In this chapter the finite element method for the electrostatic problem is analyzed. The electrostatic phenomena is well known to be dealing with stationary or slow moving charges. Such phenomena arises from the forces that the charges exert on each other. Detailed literature of electrostatics may be obtained in [12, 13]. First of all in order to formulate a problem in electrostatics, one must know the important equation called the Gauss's law, which is one of the four Maxwell's equations. If Ω is the domain and $\partial\Omega$ is the boundary, the Gauss's law is stated as "the flux of the electric displacement vector through any surface is equal to the total charge on that surface".

$$\int_{\partial\Omega} \mathbf{n} \cdot \mathcal{D} dS = \int_{\Omega} \rho_v dV \tag{2.1}$$

where $\mathcal{D}$ is the electric displacement vector and ρ_v is the volume charge density. The electric displacement vector can be written as $\mathcal{D} = \epsilon\mathcal{E}$ where ϵ is the permittivity and $\mathcal{E}$ is the electric field. The permittivity can be written as $\epsilon = \epsilon_0\epsilon_r$ where ϵ_0 is the dielectric permittivity of vacuum and ϵ_r is the relative dielectric permittivity of the medium. Now, by applying the divergence theorem on eq. (2.1) the differential form of the Gauss's law is obtained as

$$\nabla \cdot \mathcal{D} = \rho_v \tag{2.2}$$

It is known that $\nabla \times \mathcal{E}$. The electric field $\mathcal{E}$ can be rescaled and written as $\boldsymbol{E} = \epsilon_0^{1/2}\mathcal{E}$. In vector calculus any field whose curl is equal to zero (and whose gradient is not

equal to zero in some points in space), can be represented as the gradient of some other scalar field [14]. And the scalar is known as the scalar potential of the vector field. Therefore the electrostatic field can be expressed as

$$\mathbf{E} = -\nabla\phi \tag{2.3}$$

where ϕ is the electrostatic potential. It is noted that, depending on the material analyzed, the permittivity may vary. Before delving in to the finite element method for electrostatics the electrostatics boundary value problem has to be defined. Using eq. (2.2) and eq. (2.3) the Boundary Value Problem (BVP) can be written as

$$\begin{aligned} \nabla \cdot (\epsilon_r \nabla\phi) &= -\rho_v \quad \text{in} \quad \Omega \\ \phi &= \phi_D \quad \text{on} \quad \partial\Omega_D \\ \mathbf{n} \cdot (\epsilon_r \nabla\phi) &= f_N \quad \text{on} \quad \partial\Omega_N \end{aligned} \tag{2.4}$$

where Ω is the domain, $\partial\Omega_D$ is the Dirichlet boundary and $\partial\Omega_N$ is the Neumann boundary. For a two dimensional case it is shown in Figure. 3.1. It is assumed that

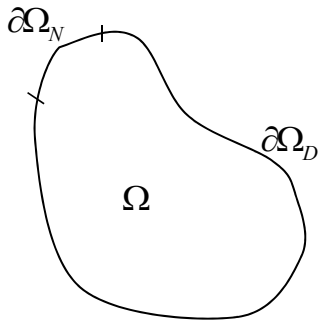

Figure 2.1: Definition of the domain and boundaries of the problem

the medium used for this problem is linear and isotropic. So that ϵ_r is taken as a scalar function of the position. If Ω consists of more than one material, this BVP should be supplemented by material interface conditions.

2.2 Weak form and finite element formulation

In this section the weak form of the problem is derived and its corresponding finite element formulation is done along with some discussion on static condensation. The

trial and test spaces for the electric potential are the H^1 space . It is the function space containing a set of functions which are, together with their first derivatives, square-integrable in Ω. Function spaces definitions are given the appendices. First the integral of the governing equation is taken over the entire domain and it is multiplied with the weighting function, so the following is obtained

$$\int_{\Omega}(\nabla\cdot(\epsilon_r\nabla\phi)wd\Omega = -\int_{\Omega}\rho_v wd\Omega \tag{2.5}$$

but in order to integrate by parts $\nabla\cdot(\epsilon_r\nabla\phi)w = \nabla\cdot[(\epsilon_r\nabla\phi)(w)] - (\epsilon_r\nabla\phi)\cdot\nabla w$

Therefore

$$\int_{\Omega}\nabla\cdot(\epsilon_r\nabla\phi w)d\Omega - \int_{\Omega}\epsilon_r\nabla\phi\cdot\nabla wd\Omega = -\int_{\Omega}\rho_v wd\Omega \tag{2.6}$$

$$\int_{\Omega}\nabla\cdot(\epsilon_r\nabla\phi w)d\Omega + \int_{\Omega}\rho_v wd\Omega = \int_{\Omega}\epsilon_r\nabla\phi\cdot\nabla wd\Omega \tag{2.7}$$

Now by using divergence theorem the above equation becomes

$$\int_{\Omega}\epsilon_r\nabla\phi\cdot\nabla wd\Omega = \int_{\partial\Omega_N}\mathbf{n}\cdot\epsilon_r\nabla\phi wd\Omega + \int_{\Omega}\rho_v wd\Omega \tag{2.8}$$

For simplicity only pure Neumann's case is considered, so the problem presents itself as to find $\phi\in H^1(\Omega)$ such that

$$\int_{\Omega}\epsilon_r\nabla\phi\cdot\nabla wd\Omega = \int_{\partial\Omega_N}\mathbf{n}\cdot\epsilon_r\nabla\phi wd\Omega + \int_{\Omega}\rho_v wd\Omega \quad \forall w\in H^1(\Omega) \tag{2.9}$$

Following the finite element method ϕ is expanded as

$$\phi\approx\phi_H = \sum_{i=1}^{M}\phi_i N_i(x,y) \tag{2.10}$$

It is known that by Galerkin's method the weighting functions are chosen as the shape functions themselves [15] i.e. $N_i(x,y)$. If eq. (2.10) is substituted in eq. (2.9),

$$\sum_{j=1}^{M}\phi_j\int_{\Omega}\epsilon_r\nabla N_j\cdot\nabla N_i d\Omega = \int_{\partial\Omega_N} n\cdot\epsilon_r\nabla\phi N_i d\Omega + \int_{\Omega}\rho_v N_i d\Omega \quad i=1,2,3...M \tag{2.11}$$

The above equation can be written as a linear system of equations as follows

$$K\Phi = r \tag{2.12}$$

where $\Phi = (\Phi_1, \Phi_2, ..., \Phi_M)^T$ and corresponding entries in K and r are given as

$$K_{ij} = \int_{\Omega} \epsilon_r \nabla N_j \cdot \nabla N_i d\Omega, \quad r_i = \int_{\partial\Omega_N} \mathbf{n} \cdot \epsilon_r \nabla \phi N_i d\Omega + \int_{\Omega} \rho_v N_i d\Omega \tag{2.13}$$

where K is the global stiffness matrix and r is the right hand side vector. In particular

$$K = \bigwedge_{e=1}^{E} k_e \tag{2.14}$$

and

$$r = \bigwedge_{e=1}^{E} r_e \tag{2.15}$$

where e represents each element, E represents the total number of elements and $\bigwedge$ represents the assembly of the element stiffness matrices. The formulation is not yet complete unless the finite element shape functions are defined, hence they are explained in the next subsection.

2.2.1 Finite element shape functions

The domain is discretized into a set of non-overlapping generic elements. Either quadrilaterals or triangles are used. The shape functions are generally defined on the reference elements and then mapped on to the general element using a linear(bilinear) mapping. Since a *hp* discretization is used, the choice of the shape function is different from the choice of the function used for mapping.

The area coordinate or the barycentric coordinates are associated with each vertex. The property of such barycentric coordinates is that they have a value of 1 at the vertex with which they are associated and zero elsewhere. The reference triangular element is shown in Fig. 2.2

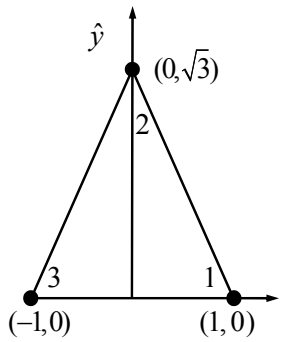

Figure 2.2: Reference triangular element

and the corresponding area coordinates are defined as

$$\lambda_1^t = \frac{1}{2\sqrt{3}}(\sqrt{3} + \sqrt{3}\hat{x} - \hat{y}) \tag{2.16}$$

$$\lambda_2^t = \frac{\hat{y}}{\sqrt{3}} \tag{2.17}$$

$$\lambda_3^t = \frac{1}{2\sqrt{3}}(\sqrt{3} - \sqrt{3}\hat{x} + \hat{y}) \tag{2.18}$$

Furthermore, for quadrilaterals, the reference element is shown in Fig. 2.3

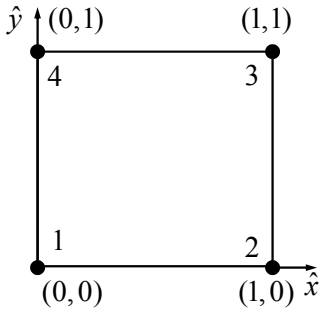

Figure 2.3: Reference quadrilateral element

and the corresponding area coordinates are defined as

$$\lambda_1^q = (1 - \hat{x})(1 - \hat{y}) \tag{2.19}$$

$$\lambda_2^q = \hat{x}(1 - \hat{y}) \tag{2.20}$$

$$\lambda_3^q = \hat{x}\hat{y} \tag{2.21}$$

$$\lambda_4^q = (1 - \hat{x})\hat{y} \tag{2.22}$$

where $\hat{x}$ and $\hat{y}$ are the reference coordinates. The area coordinates stated above correspond to the lowest order elements in both the nodal and heirarchical approaches.

Next the the higher order edge functions and interior functions employed in the code are presented. The relevant basis functions used in the code was developed by Schöberl and Zaglmayr [16]. Over a reference triangle the electrostatic potential is approximated in terms of vertex, edge and interior functions corresponding to the polynomial order p

$$\phi = \underbrace{\sum_{v=1}^{3} \phi_v \lambda_v^t}_{\text{vertex}} + \underbrace{\sum_{e=1}^{3} \sum_{i=1}^{p-1} \phi_i^e N_i^e}_{\text{edge}} + \underbrace{\sum_{i=0}^{p-3} \sum_{j=0}^{p-3} \phi_{i,j}^I N_{i,j}^I}_{\text{interior}} \tag{2.23}$$

It is to be noted at this juncture that for order $p = 1$, only the vertex shape function are needed and that the edge and the interior shape functions are not, and furthermore, the edge and interior shape functions are utilized only when orders $p > 1$ are used. The edge shape functions defined in the above equation are expanded

$$N_i^e = l_{i+1}\left(\frac{s_e}{t_e}\right)(t^e)^{i+1} \tag{2.24}$$

where $s_1 = \frac{1}{2}\hat{y}\sqrt{3} - \frac{1}{2} - \frac{1}{2}\hat{x}$, $s_2 = \frac{1}{2} - \frac{1}{2}\hat{x} - \frac{1}{2}\hat{y}\sqrt{3}$, $s_3 = \hat{x}$ and
$t_1 = \frac{1}{2} + \frac{1}{2}\hat{x} + \frac{1}{6}\hat{y}\sqrt{3}$, $t_2 = \frac{1}{2} - \frac{1}{2}\hat{x} + \frac{1}{6}\hat{y}\sqrt{3}$, $t_3 = 1 - \frac{1}{3}\hat{y}\sqrt{3}$ and l_{i+1} is the integrated Legendre polynomial of degree $i + 1$.

Also the interior shape functions are expanded as

$$N_{i,j}^I = l_{i+2}\left(\frac{S^I}{t^I}\right)(t^I)^{i+2}\lambda_3^t l_j(\lambda_3^t - \lambda_2^t - \lambda_1^t) \tag{2.25}$$

where $s_I = \lambda_2^t - \lambda_1^t$ and $t_I = \lambda_1^t + \lambda_2^t$

It is also imperative to know about the intrinsic orientation and numbering of the edges over the reference element. These data are prescribed as it is shown in Figure. 2.4.

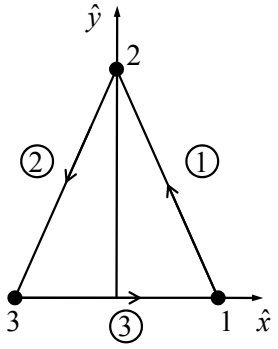

Figure 2.4: Intrinsic orientation and numbering of the edges in the triangular reference element

Now the corresponding electrostatic potential is defined over the reference quadrilateral as

$$\phi = \underbrace{\sum_{v=1}^{4} \phi_v \lambda_v^q}_{\text{vertex}} + \underbrace{\sum_{e=1}^{4} \sum_{i=1}^{p-1} \phi_i^e N_i^e}_{\text{edge}} + \underbrace{\sum_{i=0}^{p-2} \sum_{j=0}^{p-2} \phi_{i,j}^I N_{i,j}^I}_{\text{interior}} \tag{2.26}$$

The corresponding edge functions are defined as

$$N_{i,j}^I = l_{i+1}(\xi_e)\lambda_e \tag{2.27}$$

where $\lambda_1 = 1-\hat{y}$, $\lambda_2 = \hat{y}$, $\lambda_3 = \hat{x}$, $\lambda_4 = 1-\hat{x}$ and $\xi_1 = 2\hat{x}-1$, $\xi_2 = 1-2\hat{x}$, $\xi_3 = 2\hat{y}-1$, $\xi_4 = 1-2\hat{y}$

and the corresponding interior shape function is

$$N_{i,j}^I = l_{i+2}(2\hat{x}-1)l_{j+2}(2\hat{y}-1) \tag{2.28}$$

As for the triangle, the numbering and intrinsic orientation of the edges are prescribed as shown in the Figure. 2.5. Next the mapping between the reference and physical element is described.

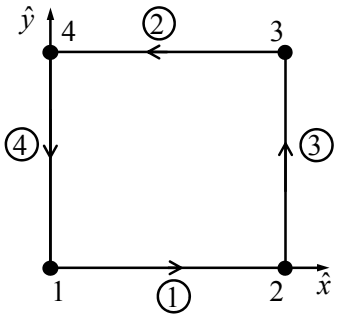

Figure 2.5: Intrinsic orientation and numbering of the edges in the quadrilateral reference element

2.2.2 Element integral evaluation

In this section the approximation of the element integrals using gauss quadrature is done. Previously the stiffness matrix and the right hand side vector were defined in eq. (2.13). Now the same equation for each element is written as

$$k_{ij}^e = \int_{\Omega_e} \epsilon_r \nabla N_i \cdot \nabla N_j d\Omega_e \tag{2.29}$$

$$r_i^e = \int_{\partial\Omega_e^N} n \cdot \epsilon_r \nabla\phi w dS + \int_{\Omega_e} \rho_v w d\Omega_e \tag{2.30}$$

Now it is important to note that integration over the physical coordinates (x,y) is needed instead of reference coordinates $(\hat{x}, \hat{y})$ where the shape functions are currently defined. So one needs to do provide a mapping from reference coordinates to physical coordinates. A linear mapping for triangle is done as it is shown in Figure. 2.6.

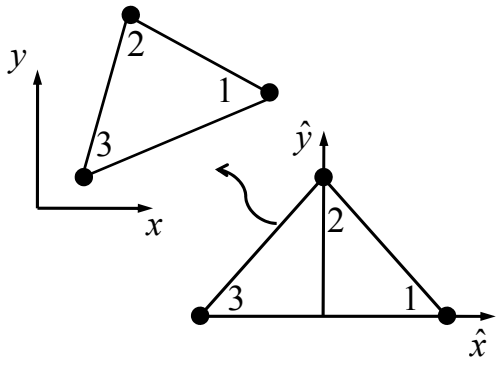

Figure 2.6: Linear mapping for triangle from reference to physical coordinates

where

$$\begin{pmatrix} x \\ y \end{pmatrix} = \sum_{i=1}^{3} \lambda_i^t \begin{pmatrix} x_i \\ y_i \end{pmatrix} \tag{2.31}$$

And a bilinear mapping is used for quadrilateral as shown in Figure. 2.7.

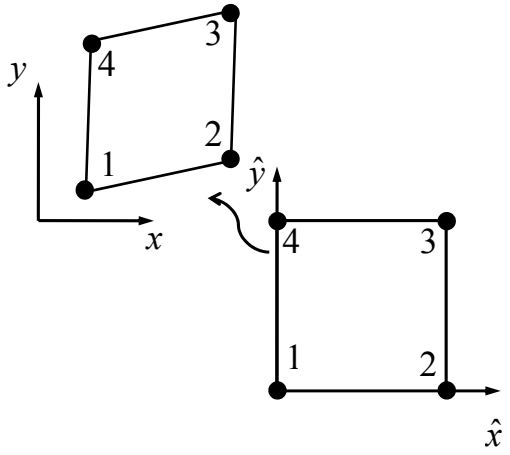

Figure 2.7: Bilinear mapping for quadrilateral from reference to physical coordinates

where

$$\begin{pmatrix} x \\ y \end{pmatrix} = \sum_{i=1}^{4} \lambda_i^q \begin{pmatrix} x_i \\ y_i \end{pmatrix} \tag{2.32}$$

After mapping of the constitutive variables of the element stiffness matrix which depend on the spatial coordinates, the element stiffness matrix looks like this

$$k_{ij}^e = \int_{\Omega_e} \epsilon_r (J^{-T} \hat{\nabla} N_i) \cdot (J^{-T} \hat{\nabla} N_j) |J| d\Omega_e \tag{2.33}$$

where J is the Jacobian matrix shown below

$$J = \begin{pmatrix} \frac{\partial x}{\partial \hat{x}} & \frac{\partial x}{\partial \hat{y}} \\ \frac{\partial y}{\partial \hat{x}} & \frac{\partial y}{\partial \hat{y}} \end{pmatrix} \tag{2.34}$$

Now by writing the element stiffness matrix by using gauss quadrature, it takes the form

$$k_{i,j}^e \approx \sum_{n=1}^{nip} \epsilon_r ((J^{-T}(\hat{x},\hat{y}) \hat{\nabla} N_i(\hat{x},\hat{y})) \cdot (J^{-T}(\hat{x},\hat{y}) \hat{\nabla} N_j(\hat{x},\hat{y})) |J(\hat{x},\hat{y})|) w_n \tag{2.35}$$

where w_n is the gauss weight and $(\hat{x}, \hat{y})$ is the gauss point and nip is the number of gauss points per element.

2.3 Static Condensation

By numbering the degrees of freedom in a consistent manner and grouping all vertex functions, edge based functions and all the vertex functions, the structure of K becomes

$$K = \begin{pmatrix} K_{VV} & K_{VE} & K_{VI} \\ K_{EV} & K_{EE} & K_{EI} \\ K_{IV} & K_{IE} & K_{II} \end{pmatrix} \tag{2.36}$$

where V is the number of non-Dirichlet points in the mesh, E is $(p-1)$ times number of non-Dirichlet edges in the mesh and $I \simeq (p-2)(p-2)$ times number of elements in the mesh. The interior degrees of freedom depend only on the value of the vertex and edge degrees of freedom for the element in consideration. This allows them to be eliminated using a process called static condensation. This process also reduces the size of the linear system. Denoting the group V, E by C, then the problem can be written as

$$K\Phi = b \tag{2.37}$$

Now expanding the terms implies

$$\begin{pmatrix} K_{CC} & K_{CI} \\ K_{IC} & K_{II} \end{pmatrix} \begin{pmatrix} \Phi_C \\ \Phi_I \end{pmatrix} = \begin{pmatrix} b_C \\ b_I \end{pmatrix} \tag{2.38}$$

Now eliminating Φ_I yields

$$\tilde{K}_{CC}\Phi = \tilde{b}_C \tag{2.39}$$

where

$$\tilde{K}_{CC} = K_{CC} - K_{CI}K_{II}^{-1}K_{IC} \tag{2.40}$$

$$\tilde{b}_C = b_C - K_{CI}K_{II}^{-1}b_I \tag{2.41}$$

Now Φ_I can be found using

$$\Phi_I = K_{II}^{-1}b_I - K_{II}^{-1}K_{IC}\Phi_C \tag{2.42}$$

2.4 Analytical solution for benchmark example

The rectangular trough of infinite length in the z direction is taken to be the electrostatic benchmark problem. It is described in Figure. 2.8. It is noted that it has singularities in the top corners due to adjacent edges having Dirichlet boundary conditions.

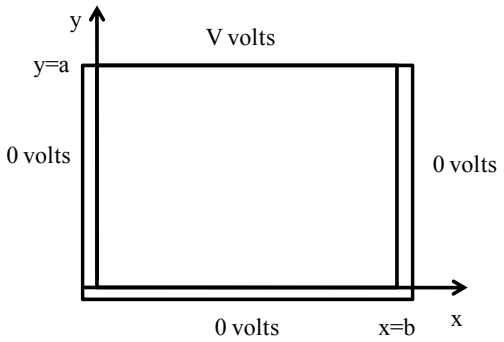

Figure 2.8: Electrostatics problem - conducting trough

According to [17], the following procedure is followed to obtain the analytical solution for the BVP. If the permittivity ϵ_r is kept constant over the whole region with no variation in the z direction, the governing equation for the problem can be written in terms of the x and y coordinates as

$$\frac{\partial^2 \phi}{\partial x^2} + \frac{\partial^2 \phi}{\partial y^2} = 0 \tag{2.43}$$

Using the method separation of variables, ϕ can be written as

$$\phi = X(x)Y(y) \tag{2.44}$$

Therefore,

$$YX'' + XY'' = 0 \tag{2.45}$$

$$-\frac{X''}{X} = \frac{Y''}{Y} = \lambda \tag{2.46}$$

where λ is a constant since the left hand side (LHS) is a function of X and right hand side (RHS) is a function of Y only. Considering the three cases $\lambda = 0$, $\lambda < 0$

and $\lambda > 0$, the problem can be solved. First put $\lambda = 0$, then from eq. (2.45)

$$X = Ax + B \tag{2.47}$$

Now the boundary condition reads $X(x = 0) = 0$, $X(x = b) = 0$. Therefore

$$X(x = 0) = B = 0 \tag{2.48}$$

$$X(x = b) = Ab = 0 \Rightarrow A = 0 \tag{2.49}$$

Therefore it is inferred that X is zero. But it cannot be so the case and so $\lambda \neq 0$. Considering the next case $\lambda < 0$, putting $\lambda = -\alpha^2$ implies

$$\frac{d^2X}{dx^2} - \alpha^2 X = 0 \tag{2.50}$$

Therefore after integration the solution is

$$X = A_1 e^{\alpha x} + A_2 e^{-\alpha x} \tag{2.51}$$

Since it is known that

$$\sinh \alpha x = \frac{e^{\alpha x} - e^{-\alpha x}}{2} \tag{2.52}$$

$$\cosh \alpha x = \frac{e^{\alpha x} + e^{-\alpha x}}{2} \tag{2.53}$$

Therefore X becomes

$$X = B_1 \cosh \alpha x + B_2 \sinh \alpha x \tag{2.54}$$

where $B_1 = A_1 + A_2$ and $B_2 = A_1 - A_1$. Now the boundary condition reads $X(x = 0) = 0$, $X(x = b) = 0$. Applying the boundary condition it is seen that

$$X(x = 0) = B_1 = 0 \tag{2.55}$$

$$X(x = b) = B_2 \sinh \alpha b = 0 \Rightarrow B_2 = 0 \tag{2.56}$$

However, once again $X = 0$, so this case can be ignored. Therefore for obtaining the correct solution λ has to be greater than zero. Setting λ as α^2 implies

$$\frac{d^2X}{dx^2} + \alpha^2 X = 0 \tag{2.57}$$

Therefore, the solution becomes

$$X = A_1 \cos \alpha x + A_2 \sin \alpha x \tag{2.58}$$

Again the boundary condition read $X(x = 0) = 0$, $X(x = b) = 0$, so $A_1 = 0$ and $\sin \alpha b = 0$, where α is expressed as

$$\alpha = \frac{n\pi}{b}, \quad n = 1, 2, 3, 4... \tag{2.59}$$

It is to be noted that if $n = 0$, the equation once again leads to incorrect solution. Also if n is negative it gives the same solution as when it is positive. Therefore

$$\lambda = \alpha^2 = \frac{n^2\pi^2}{b^2}, \quad n = 1, 2, 3, 4... \tag{2.60}$$

Next $Y'' - \lambda Y = 0$ can be solved in the same lines as X and thus solution is found to be dependant on

$$Y_n = B_n \sinh \frac{n\pi}{b} \tag{2.61}$$

Therefore there are n such solutions, ϕ_n, which can be written as

$$\phi_n = C_n \sin \frac{n\pi x}{b} \sinh \frac{n\pi y}{b} \tag{2.62}$$

In general a particular solution is given by a linear combination of Φ_n

$$\phi = \sum_{n=1}^{\infty} C_n \sin \frac{n\pi x}{b} \sinh \frac{n\pi y}{b} \tag{2.63}$$

Now the boundary condition reads $\phi(x, a) = \mathrm{V}$. Then C_n is found to be

$$C_n = \begin{cases} \dfrac{4V}{n\pi \sinh \dfrac{n\pi a}{b}} & n \ \ is \ \ odd \\ 0 & n \ \ is \ \ even \end{cases} \tag{2.64}$$

In the problem if $\mathrm{V} = 1$, then the potential ϕ can be written as

$$\phi = \frac{4}{\pi} \sum_{n=1,3,5}^{\infty} \frac{\sin \dfrac{n\pi x}{b} \sinh \dfrac{n\pi y}{b}}{n \sinh \dfrac{n\pi a}{b}} \tag{2.65}$$

2.5 Numerical results and discussion

The first step involves a pre processing stage, where the mesh is generated. Firstly a uniform mesh with triangles is used. A typical mesh of spacing $h = 0.1$ is shown in Figure. 2.9.

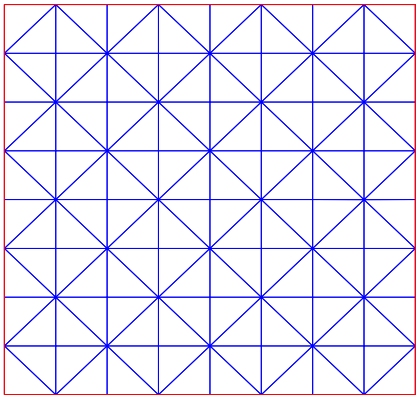

Figure 2.9: Uniform triangulated mesh

Next at the solver stage, it is reminded that the finite element method with *hp* discretization is used to solve the electrostatics BVP. The details of the formulation were shown earlier. The solution is obtained using the finite element method and the sets of results obtained are shown subsequently and they are qualitatively and quantitatively observed and conclusions are drawn based on different factors. Considering a uniform meshes with elements of uniform order, the contour plot of the electrostatic potential is shown in the Figure. 2.10.

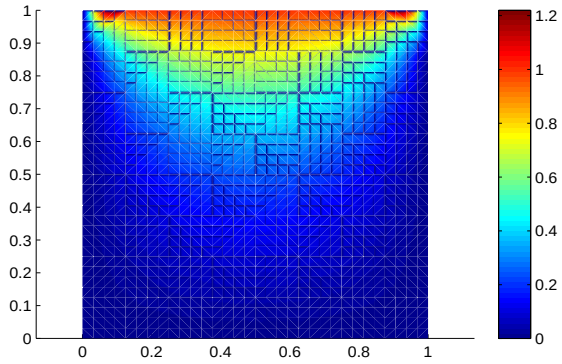

Figure 2.10: Contour plot of the electrostatic potential

It can be observed that there are two singularities present at the top two corners. The vector plot of the gradient of electrostatic potential is shown in Figure. 2.11.

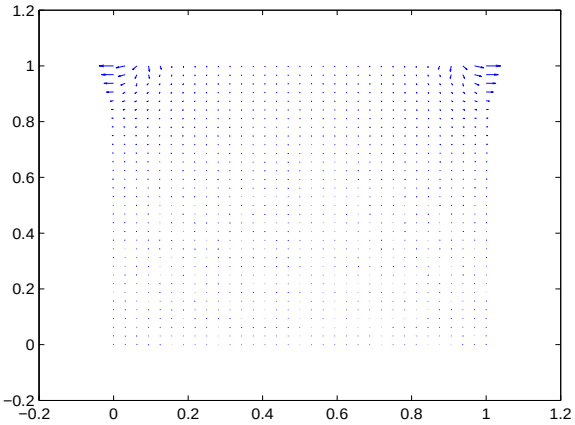

Figure 2.11: Vector plot of the gradient of the electrostatic potential

In order to show the accuracy of the results, the error has to be measured. The L_2 norm of the error is used for representing the error between exact values of the potential and the numerical value [15]. The norms are defined in the appendix. In order to know the rates of convergence for h, p and hp-refinements, simulations are performed and the results are shown in the following figures. A mesh with

triangular discretization is used and Figure. 2.12 shows the L_2 norm of the error in the electrostatic potential while performing h refinement for orders 1, 2, 3 and 4.

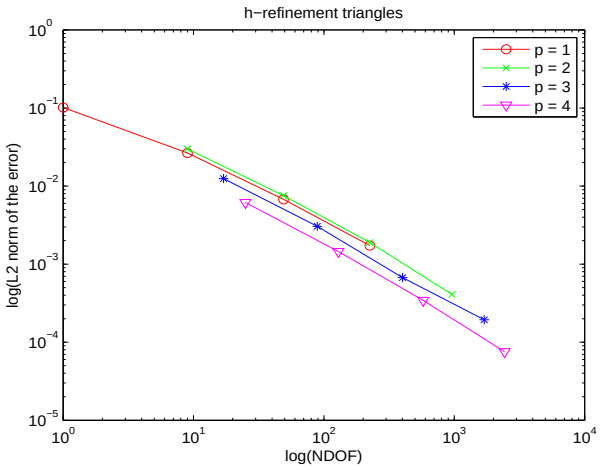

Figure 2.12: Convergence plot for h refinement

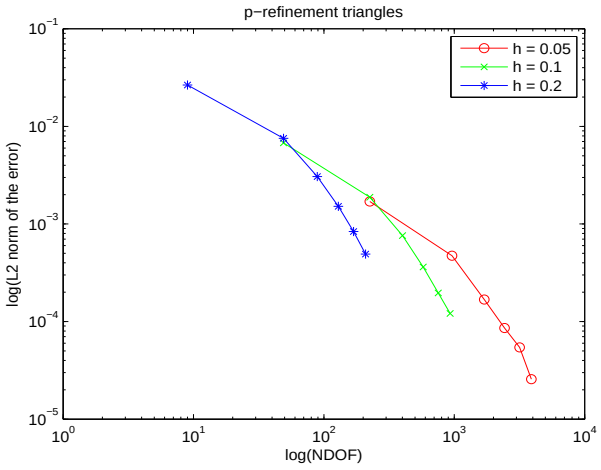

Figure 2.13: Convergence plot for h refinement

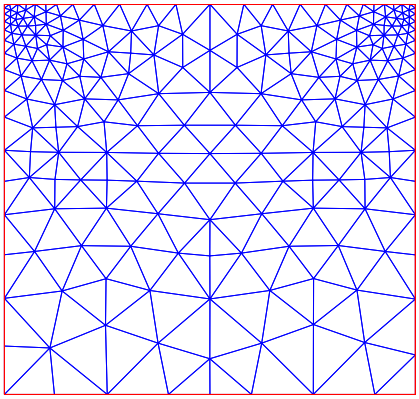

Figure 2.14: Non uniform mesh for the given electrostatics problem

It is observed that the convergence is algebraic since the convergence curves are straight lines. Next the Figure. 2.13 shows the same error but now with p refinement for mesh spacings $h = 0.05,\ 0.1$ and 0.2. The convergence appears to be exponential but the error drops to the same level as it does during h refinement. This trend is expected since there are two singularities present at the top two corners. However, if h and p refinements are used simultaneously with a non uniform mesh, then the convergence is expected to be faster. The non uniform mesh is shown in Figure. 2.14. It is observed that the error in this case dropped to the orders of 10^{-6} at the first step i.e. for the order 2. However the simulation could not be proceeded further since the number of terms in the infinite series of the analytical solution exceeded the threshold of computing power in the stand alone machine in usage. Since for order 2 the error has dropped down so low, it can be concluded that exponential convergence would have been achieved. Thus it can be ascertained that, in the the presence of singularities, a combination of h and p refinement would result in exponential convergence. Next chapter deals with the analysis of the fluid mechanics problem.

Chapter 3

Analysis of the fluid field

3.1 Introduction

In this chapter the finite element method with *hp* discretization will be applied for the solution of a Stokes flow problem. Initially the governing equations for Stokes flow are discussed. Next the standard mixed formulation is explained followed by two different solution strategies, namely the penalty function formulation and the mixed formulation with slight compressibility. Benchmarking simulations are done for three cases namely the Poiseiulle's flow through a duct, a problem with a prescribed body force and for a lid driven cavity problem.

3.2 Governing Equations and problem definition

First the Navier-Stokes equations are introduced. The domain to be analyzed can be considered as Ω and the boundary to be $\Gamma = \partial\Omega$ which is assumed to be a regular and continuous surface. The Navier Stokes equations for a time dependant viscous fluid flow problem is given as follows.

$$\rho(\mathbf{u_t} + (\mathbf{u}\cdot\nabla)\mathbf{u}) - \mu\nabla^2\mathbf{u} - \mu\nabla(\nabla\cdot\mathbf{u}) + \nabla p \;=\; \rho\mathbf{b} \quad \text{in} \quad \Omega \tag{3.1}$$

where $\mathbf{v}$ is the velocity, ρ is the density, μ is the dynamic viscosity and $\mathbf{b}$ is the body force. If incompressible flow is considered, then

$$\nabla\cdot\mathbf{u} \;=\; 0 \quad \text{in} \quad \Omega \tag{3.2}$$

Now, substituting eq. (3.2) in eq. (3.1) results in

$$\rho(\mathbf{u_t} + (\mathbf{u}\cdot\nabla)\mathbf{u}) - \mu\nabla^2\mathbf{u} + \nabla p = \rho\mathbf{b} \tag{3.3}$$

Since the flow considered is steady and since the Stokes flow involves highly viscous flow, the time term $\mathbf{u_t}$ and the convective term $(\mathbf{v}\cdot\nabla)\mathbf{v}$ in eq. (3.3) can be ignored and the the resulting equations are the time independent Stokes flow governing equations

$$\begin{aligned} -\mu\nabla^2\mathbf{u} + \nabla p &= \mathbf{f} \quad \text{in} \quad \Omega \\ \nabla \cdot \mathbf{u} &= 0 \quad \text{in} \quad \Omega \end{aligned} \tag{3.4}$$

In the eq. (3.4), the right hand side term can be given as $\mathbf{f} = \rho\mathbf{b}$, representing the body force. The eq. (3.2) is still required as a constraint. This form of the equations is known as the velocity pressure form. An alternative form would be the stress divergence form, which would be used later.

3.2.1 Strong form of the problem

The Boundary Value Problem (BVP) for the Stokes flow in the velocity pressure form can be written as

$$\begin{aligned} -\mu\nabla^2\mathbf{u} + \nabla p &= \mathbf{f} && \text{in} \quad \Omega \\ \nabla \cdot \mathbf{u} &= 0 && \text{in} \quad \Omega \\ \mathbf{u} &= \mathbf{u}_D && \text{on} \quad \partial\Omega_D \\ \mathbf{t} &= -\mathbf{n}p + \mu(\mathbf{n}\cdot\nabla)\mathbf{u} && \text{on} \quad \partial\Omega_N \end{aligned} \tag{3.5}$$

where $\mathbf{t}$ is the traction, $\mathbf{u}_D$ is the velocity at the Dirichlet boundary, Ω is the domain, $\partial\Omega_D$ is the Dirichlet boundary and $\partial\Omega_N$ is the Neumann boundary. The problem domain is shown in Figure. 3.2.1.

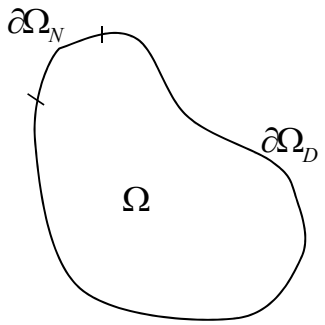

Figure 3.1: Definition of the domain and boundaries of the problem

Three different formulations are presented subsequently. The first formulation is the standard mixed formulation where the incompressibility constraint is strictly imposed and the solutions are obtained for both the velocities and the pressure. The next formulation is the penalty function formulation where the the fluid is treated as nearly being incompressible and solution is obtained for the velocities, with pressure being computed using a post processing setup. The third formulation is a mixed formulation, which is also a penalty type method, where the fluid is treated as being nearly incompressible, however the solution obtained for both velocities and the pressure. Next a brief discussion on standard mixed formulation is presented.

3.3 Standard mixed formulation

The standard mixed formulation is only briefly discussed since the work in the thesis mostly involves the use of other methods, which are discussed after this section. In the standard mixed formulation for Stokes flow, solutions are obtained for both velocity and pressure, while maintaining strict incompressibility constraint. The strong form of the problem is written in eq. (3.5). Next the weak form of the problem is presented.

3.3.1 Weak form of the problem

The trial and test spaces for the velocity and the pressure are defined as

$$\mathbf{V} = \{\mathbf{u} \in (\boldsymbol{H}^1(\Omega)), \mathbf{u} = \mathbf{u}_D \text{ on } \partial\Omega_D\} \tag{3.6}$$

$$\mathbf{W} = \{\mathbf{w} \in (\boldsymbol{H}^1(\Omega)), \mathbf{w} = \mathbf{0} \text{ on } \partial\Omega_D\} \tag{3.7}$$

$$Z = \{p \in L^2(\Omega), \int_\Omega p d\Omega = 0\} \tag{3.8}$$

where $\boldsymbol{H}^1$ is the function space whose components are functions which are, together with their first derivatives, square-integrable in Ω and L^2 is the function space containing a set of functions which are square-integrable in Ω.Function spaces definitions are given the appendices. From the strong form of the problem previously defined before, its integral is taken over the entire domain Ω and multiplied with the velocity

weighting function $\mathbf{w}$ and the pressure weighting functions q which results as

$$\int_\Omega -\mu(\nabla^2\mathbf{u})\cdot\mathbf{w}d\Omega + \int_\Omega \mathbf{w}\cdot\nabla p d\Omega = \int_\Omega \mathbf{w}\cdot\mathbf{f}d\Omega \tag{3.9}$$

$$\int_\Omega q(\nabla\cdot\mathbf{u})d\Omega = 0 \tag{3.10}$$

The eq. (3.9) can be simplified as follows

$$\int_\Omega -\mu(\nabla\cdot\nabla\mathbf{u})\cdot\mathbf{w}d\Omega + \int_\Omega \mathbf{w}\cdot\nabla p d\Omega = \int_\Omega \mathbf{w}\cdot\mathbf{f}d\Omega \tag{3.11}$$

but it is known that

$$\nabla\cdot((\nabla\mathbf{u})\mathbf{w}) = (\nabla\cdot\nabla\mathbf{u})\cdot\mathbf{w} + (\nabla\mathbf{w}:\nabla\mathbf{u}) \tag{3.12}$$

and

$$\nabla\cdot(\mathbf{w}p) = \mathbf{w}\cdot\nabla p + p(\nabla\cdot\mathbf{w}) \tag{3.13}$$

Therefore eq. (3.11) becomes

$$\int_\Omega \nabla\mathbf{w}:\mu\nabla\mathbf{u}d\Omega - \int_\Omega \mu\nabla\cdot((\nabla\mathbf{u})\mathbf{w})d\Omega + \int_\Omega \nabla\cdot(\mathbf{w}p)d\Omega - \int_\Omega p(\nabla\cdot\mathbf{w})d\Omega = \int_\Omega \mathbf{w}\cdot\mathbf{f}d\Omega \tag{3.14}$$

Applying divergence theorem to the corresponding terms in eq. (3.14) implies

$$\int_\Omega \nabla\mathbf{w}:\mu\nabla\mathbf{u}d\Omega - \int_\Omega p(\nabla\cdot\mathbf{w})d\Omega = \int_\Omega \mathbf{w}\cdot\mathbf{f} + \int_{\partial\Omega_N} \mathbf{w}\cdot\mathbf{t}d\Omega \tag{3.15}$$

where Ω_N is the Neumann boundary and $\mathbf{t}$ is the tractions, which is defined as

$$\mathbf{t} = -\mathbf{n}p + \mu(\mathbf{n}\cdot\nabla)\mathbf{u} \tag{3.16}$$

So the weak form can be stated as Find $\mathbf{u}\in\mathbf{V}$ and $p\in Z$ such that $\forall\ \mathbf{w}\in\mathbf{W}$ and $q\in Z$

$$a(\mathbf{u},\mathbf{w}) - (\nabla\cdot\mathbf{w},p)_\Omega = (\mathbf{w},\mathbf{f})_\Omega + (\mathbf{w},\mathbf{t})_{\partial\Omega_N} \tag{3.17}$$

$$b(\mathbf{u},q) = 0 \tag{3.18}$$

where

$$a(\mathbf{w},\mathbf{u}) = \int_{\Omega} \nabla\mathbf{w} : \mu\nabla\mathbf{u} \tag{3.19}$$

$$(\nabla\cdot\mathbf{w},p)_{\Omega} = \int_{\Omega} p(\nabla\cdot\mathbf{w})d\Omega \tag{3.20}$$

$$b(\mathbf{u},q) = \int_{\Omega} q(\nabla\cdot\mathbf{u})d\Omega \tag{3.21}$$

$$(\mathbf{w},\mathbf{f})_{\Omega} = \int_{\Omega} \mathbf{w}\cdot\mathbf{f}d\Omega \tag{3.22}$$

$$(\mathbf{w},\mathbf{t})_{\partial\Omega_N} = \int_{\partial\Omega_N} \mathbf{w}\cdot\mathbf{t}d\Omega \tag{3.23}$$

3.3.2 Galerkin formulation

The Galerkin counterpart of the weak form can be given as Find $\mathbf{u}_{hp} \in \mathbf{V}_{hp}$ and $p_{hp} \in Z_{hp}$ such that $\forall\ \mathbf{w}_{hp} \in \mathbf{W}_{hp}$ and $q_{hp} \in Z_{hp}$

$$a(\mathbf{u}_{hp},\mathbf{w}_{hp}) - (\nabla\cdot\mathbf{w}_{hp},p_{hp}) = (\mathbf{w}_{hp},\mathbf{f}) + (\mathbf{w}_{hp},\mathbf{t}) \tag{3.24}$$

$$b(\mathbf{u}_{hp},q_{hp}) = 0 \tag{3.25}$$

where subscript hp denotes the descretization and where $\mathbf{V}_{hp} \subset \mathbf{V}$, $\mathbf{W}_{hp} \subset \mathbf{W}$ and $Z_{hp} \subset Z$. In the standard mixed formulation, there is a stability condition to be satisfied, known as the Babuska-Brezzi condition [2]. For the condition to be satisfied, and for the flow to be stable, there must be a two order difference in approximation of velocity and pressure. Further details of standard mixed formulation can be found in [15] and in [2].

The standard mixed formulation is not pursued further due to time limitations the thesis. Other formulations which are are used in the thesis are discussed in the following sections.

3.4 Equivalence between elasticity equation and Stokes equation

Before introducing the penalty function formulation and the mixed formulation, the equivalence between linear elasticity equation for an incompressible material and the Stokes flow equation is established. The governing equation for linear elasticity is stated as

$$\nabla \cdot \sigma + \mathbf{f} = 0 \quad \text{in} \quad \Omega \tag{3.26}$$

where σ is the stress in the material and $\mathbf{f}$ is the body force. If the material is incompressible, the displacements must also satisfy $\nabla \cdot \mathbf{u} = 0$. The constitutive equation for incompressible linear elasticity can be stated [15] as

$$\sigma = -pI + 2\mu\nabla^S\mathbf{u} \tag{3.27}$$

where p is the hydrostatic pressure, μ is the shearing modulus, $\nabla^S\mathbf{u}$ is the symmetric component of the gradient of displacements. Substituting eq. (3.27) in eq. (3.26) results in the following equation

$$-\mu\nabla^2\mathbf{u} + \nabla p = \mathbf{f} \tag{3.28}$$

Considering eq. (3.4) and eq. (3.28), it is observed that, these equations are *identical* except for the definitions of the variables. If the variable μ is taken to be the viscosity of the fluid and if the variable $\mathbf{u}$ is taken to be the velocity of the fluid, then the eq. (3.4) is called the velocity pressure form and the eq. (3.26) is known as the stress divergence form of the Stokes flow governing equations [2].

The requirement that $\nabla \cdot \mathbf{u} = 0$ is rarely imposed in the linear elasticity and instead the concept of almost incompressible materials is often considered. In this case, material with Poisson's ratio close to 0.5 are considered. These materials have finite but small value of $\nabla \cdot \mathbf{u}$. In the limiting case of $\nu = 0.5$, $\nabla \cdot \mathbf{u} = 0$. Thus by appropriate choice of the Poisson's ratio, the solution of linear elasticity can be viewed as a regularized Stokes flow solver which has a property that $\nabla \cdot \mathbf{u} \to 0$ as $\nu \to 0.5$. This is described in detail in the next section.

3.5 Penalty function formulation

In the penalty function formulation, the constitutive equation given in eq. (3.27) is written as

$$\sigma^\lambda = -p^\lambda I + 2\mu\nabla^S \mathbf{u}^\lambda \tag{3.29}$$

in which

$$p^\lambda = -\lambda\nabla\cdot\mathbf{u}^\lambda \tag{3.30}$$

where $\lambda > 0$ acts as a regularization parameter. This parameter is related to the Poisson's ratio in a way that, as $\lambda \to \infty$, $\nu \to 0.5$. Thus the incompressibility condition can therefore be dropped from the strong form of the problem. The strong form of the problem can be written for the penalty function formulation of Stokes flow as

$$\begin{aligned} \nabla\cdot\sigma^\lambda + \mathbf{f} &= 0 \quad \text{in} \quad \Omega \\ \mathbf{u}^\lambda &= \mathbf{u}_D \quad \text{on} \quad \partial\Omega_D \\ \sigma^\lambda\cdot\mathbf{n} &= \mathbf{t} \quad \text{on} \quad \partial\Omega_N \end{aligned} \tag{3.31}$$

According to [18], as $\lambda \to \infty$ $\mathbf{u}^\lambda \to \mathbf{u}$ in $\mathbf{H}^1$ and $p^\lambda \to p$ in L_2. So if λ is selected sufficiently large then $\mathbf{u}^\lambda$ and p^λ differ negligibly from $\mathbf{u}$ and p for the Stokes flow problem [18]. The advantage of penalty function method is that the additional unknown p is eliminated and the necessity for solving the incompressibility condition is removed. Numerically it is simpler to implement as the problem requires only $\mathbf{u}$ to be discretized. In this section it is convinient to omit the λ superscripts.

3.5.1 Weak form of the problem

The trial and test spaces for the velocities are defined as

$$\mathbf{V} = \{\mathbf{u} \in (\boldsymbol{H}^1(\Omega)), \mathbf{u} = \mathbf{u}_D \ \text{ on } \ \partial\Omega_D\} \tag{3.32}$$

$$\mathbf{W} = \{\mathbf{w} \in (\boldsymbol{H}^1(\Omega)), \mathbf{w} = \mathbf{0} \ \text{ on } \ \partial\Omega_D\} \tag{3.33}$$

From the strong form of the problem defined before in eq. (3.31), its integral is taken over the entire domain Ω and multiplied with the velocity weighting function

$\mathbf{w}$ which results as

$$-\int_{\Omega} \mathbf{w} \cdot (\nabla \cdot \sigma) d\Omega = \int_{\Omega} \mathbf{w} \cdot \mathbf{f} d\Omega \tag{3.34}$$

for integrating by parts, the term $\mathbf{w} \cdot (\nabla \cdot \sigma)$ can be written as

$$\mathbf{w} \cdot (\nabla \cdot \sigma) = \nabla \cdot (\sigma \mathbf{w}) - \nabla \mathbf{w} : \sigma \tag{3.35}$$

therefore eq. (3.34) can be re-written as

$$\int_{\Omega} \nabla \mathbf{w} : \sigma d\Omega = \int_{\Omega} \mathbf{w} \cdot \mathbf{f} d\Omega + \int_{\Omega} \nabla \cdot (\sigma \mathbf{w}) d\Omega \tag{3.36}$$

but using divergence theorem and the fact that $\mathbf{n} \cdot \sigma = \mathbf{t} on \partial\Omega_N$. Therefore eq. (3.36) can be written as

$$\int_{\Omega} \nabla \mathbf{w} : \sigma d\Omega = \int_{\Omega} \mathbf{w} \cdot \mathbf{f} d\Omega + \int_{\partial\Omega_N} \mathbf{w} \cdot \mathbf{t} d\Omega \tag{3.37}$$

Now using the constitutive equation from eq. (3.27), the variational problem could be written as

$$\int_{\Omega} \nabla^s \mathbf{w} : C : \nabla^s \mathbf{v} - \int_{\Omega} \lambda (\nabla \cdot \mathbf{u})(\nabla \cdot \mathbf{w}) d\Omega = \int_{\Omega} \mathbf{w} \cdot \mathbf{f} d\Omega + \int_{\partial\Omega_N} \mathbf{w} \cdot \mathbf{t} \Omega \tag{3.38}$$

where C is the fourth order constitutive tensor called the viscosity matrix. Now, the weak form of the BVP is stated as Find $\mathbf{u} \in \mathbf{V}$ such that $\forall\ \mathbf{w} \in \mathbf{V}$

$$c(\mathbf{w}, \mathbf{u}) = (\mathbf{w}, \mathbf{f})_{\Omega} + (\mathbf{w}, \mathbf{t})_{\partial\Omega_N} \tag{3.39}$$

where

$$c(\mathbf{w}, \mathbf{u}) = \int_{\Omega} \nabla^s \mathbf{w} : C : \nabla^s \mathbf{u} \partial\Omega - \int_{\Omega} \lambda (\nabla \cdot \mathbf{u})(\nabla \cdot \mathbf{w}) d\Omega \tag{3.40}$$

$$(\mathbf{w}, \mathbf{f})_{\Omega} = \int_{\Omega} \mathbf{w} \cdot \mathbf{f} d\Omega \tag{3.41}$$

$$(\mathbf{w}, \mathbf{t})_{\partial\Omega_N} = \int_{\partial\Omega_N} \mathbf{w} \cdot \mathbf{t} d\Omega \tag{3.42}$$

3.5.2 Galerkin formulation and matrix problem

The Galerkin's counterpart of the weak formulation can be given as Find $\mathbf{u}_{hp} \in \mathbf{V}_{hp}$ such that $\forall\ \mathbf{w}_{hp} \in \mathbf{W}_{hp}$

$$c(\mathbf{u}_{hp}, \mathbf{w}_{hp}) = (\mathbf{w}_{hp}, \mathbf{f})_{\Omega} + (\mathbf{w}_{hp}, \mathbf{t})_{\partial\Omega_N} \tag{3.43}$$

where $\mathbf{V}_{hp} \subset \mathbf{V}$ and $\mathbf{W}_{hp} \subset \mathbf{W}$. Following the finite element method, $\mathbf{u}_{hp}$ can be expanded as

$$\mathbf{u}_{hp} = \sum_{i=1}^{M} N_i(x, y)\mathbf{u}_i \tag{3.44}$$

where the M is the number of basis functions. The weighting functions are chosen as the shape functions themselves. Now the matrix problem reads as

$$KU = \mathbf{f} \tag{3.45}$$

where

$$K = \bigwedge_{e=1}^{E} k^{(e),ab} \tag{3.46}$$

where e represents each element, E represents the total number of elements, $\bigwedge$ represents the assembly of the element stiffness matrices and $k^{(e),ab}$ represents the element stiffness matrix, which can be written as

$$k^{(e),ab} = \int_{\Omega^e} B^{a^T} D B^b d\Omega \tag{3.47}$$

where B is given as

$$B^a = \begin{pmatrix} \dfrac{\partial N^a}{\partial x} & 0 \\ 0 & \dfrac{\partial N^a}{\partial y} \\ \dfrac{\partial N^a}{\partial y} & \dfrac{\partial N^a}{\partial x} \end{pmatrix} \tag{3.48}$$

and the material properties matrix D [15] is given as

$$D = D_\lambda + D_\mu \tag{3.49}$$

where D_λ and D_μ are given as

$$D_\lambda = \lambda \begin{pmatrix} 1 & 1 & 0 \\ 1 & 1 & 0 \\ 0 & 0 & 0 \end{pmatrix} \tag{3.50}$$

$$D_\mu = \mu \begin{pmatrix} 2 & 0 & 0 \\ 0 & 2 & 0 \\ 0 & 0 & 1 \end{pmatrix} \tag{3.51}$$

Therefore, it can be seen that the k_e can be written as

$$k_e = k_\lambda^{(e),ab} + k_\mu^{(e),ab} \tag{3.52}$$

where

$$k_\lambda^{(e),ab} = \int_{\Omega^e} B^{a^T} D_\lambda B^b d\Omega \tag{3.53}$$

$$k_\mu^{(e),ab} = \int_{\Omega^e} B^{a^T} D_\mu B^b d\Omega \tag{3.54}$$

It is because of the fact that $\dfrac{\lambda}{\mu} \gg 1$ the k_e^λ term tends to be large and it attempts to maintain the volumetrically stiff behavior [15]. And this contributes to the phenomenon of volumetric locking. This is alleviated by the use of a *hp* discretization. Furthermore the relevant basis functions used are the same as in the electrostatics problem, which were taken from Schöberl and Zaglmayr [16]. The numerical benchmark results for this method will be shown subsequently. Next a mixed finite element approach of the penalty formulation of Stokes flow is presented.

3.6 Mixed approach for the penalty formulation of Stokes flow

This is a mixed approach for the elasticity system. Equivalence between penalty function formulation and elasticity system as $\nu \to 0.5$ is discussed already in the previous sections. In this method the problem is solved for both velocity and pressure,

therefore weighting and trial solution spaces are introduced for the pressures also. This method can be viewed as a perturbed Lagrangian method [19]. The pressure variable is introduced as an independent unknown. The pressure variable p can be interpreted as the hydrostatic pressure only in the incompressible case [15] as

$$p = -\mathrm{tr}(\sigma)/2 \tag{3.55}$$

If a compressible case is considered, according to the constitutive equation given in eq. (3.27),

$$-\mathrm{tr}(\sigma)/2 = -(\lambda + 2\mu/2)\nabla \cdot \mathbf{u} \tag{3.56}$$

where $\mathbf{u}$ is the velocity but $\lambda + 2\mu/2$ can be viewed as the bulk modulus κ. Thus if the flow is nearly incompressible, $\lambda \approx \kappa$. In view of the above discussion the strong form of the problem in this formulation can be written as

$$\begin{aligned} \nabla \cdot \sigma + \mathbf{f} &= 0 \quad \text{in} \quad \Omega \\ \nabla \cdot \mathbf{u} + p/\kappa &= 0 \quad \text{in} \quad \Omega \\ \mathbf{u} &= \mathbf{u}_D \quad \text{on} \quad \partial\Omega_D \\ \sigma \cdot \mathbf{n} &= \mathbf{t} \quad \text{on} \quad \partial\Omega_N \end{aligned} \tag{3.57}$$

3.6.1 Weak form of the problem

The trial and test spaces for the velocities and pressure are defined as

$$\mathbf{V} = \{\mathbf{u} \in (\boldsymbol{H}^1(\Omega)), \mathbf{u} = \mathbf{u}_D \ \text{ on } \ \partial\Omega_D\} \tag{3.58}$$

$$\mathbf{W} = \{\mathbf{w} \in (\boldsymbol{H}^1(\Omega)), \mathbf{w} = \mathbf{0} \ \text{ on } \ \partial\Omega_D\} \tag{3.59}$$

$$Z = \{p \in L^2(\Omega)\} \tag{3.60}$$

$\mathbf{w} \in \mathbf{W}$ is the weighting function for the velocity and $q \in Z$ is the weighting function for the pressure. The weak form is obtained as follows.

$$-\int_\Omega \mathbf{w} \cdot (\nabla \cdot \sigma) d\Omega = \int_\Omega \mathbf{w} \cdot \mathbf{f} d\Omega \tag{3.61}$$

$$-\int_{\Omega} q(\nabla \cdot \mathbf{v} + p/\kappa) d\Omega = 0 \tag{3.62}$$

Considering eq. (3.61), for integrating by parts, the term $\mathbf{w}(\nabla \cdot \sigma)$ can be written as

$$\mathbf{w} \cdot (\nabla \cdot \sigma) = \nabla \cdot (\sigma \mathbf{w}) - \nabla \mathbf{w} : \sigma \tag{3.63}$$

therefore eq. (3.61) can be re-written as

$$\int_{\Omega} \nabla \mathbf{w} : \sigma d\Omega = \int_{\Omega} \mathbf{w} \cdot \mathbf{f} d\Omega + \int_{\Omega} \nabla \cdot (\sigma \mathbf{w}) d\Omega \tag{3.64}$$

but using divergence theorem and the fact that $\mathbf{n} \cdot \sigma = \mathbf{t} \;\; on \;\; \partial\Omega_N$. Therefore eq. (3.64) can be written as

$$\int_{\Omega} \nabla \mathbf{w} : \sigma d\Omega = \int_{\Omega} \mathbf{w} \cdot \mathbf{f} d\Omega + \int_{\partial\Omega_N} \mathbf{w} \cdot \mathbf{t} d\Omega \tag{3.65}$$

Now using eq. (3.27), which is the constitutive law the variational problem can be written as

$$\int_{\Omega} \nabla^s \mathbf{w} : C : \nabla^s \mathbf{v} - \int_{\Omega} p \nabla \cdot \mathbf{w} d\Omega = \int_{\Omega} \mathbf{w} \cdot \mathbf{f} d\Omega + \int_{\partial\Omega_N} \mathbf{w} \cdot \mathbf{t} \Omega \tag{3.66}$$

Now the weak form of the BVP is stated as follows: Find $\mathbf{u} \in \mathbf{V}$ and $p \in Z$ such that $\forall \; \mathbf{w} \in \mathbf{W}$ and $q \in Z$

$$d(\mathbf{u}, \mathbf{w}) - (\nabla \cdot \mathbf{w}, p)_{\Omega} = (\mathbf{w}, \mathbf{f})_{\Omega} + (\mathbf{w}, \mathbf{t})_{\partial\Omega_N} \tag{3.67}$$

$$-(q, \nabla \cdot \mathbf{u} + p/\kappa)_{\Omega} = 0 \tag{3.68}$$

where

$$d(\mathbf{w}, \mathbf{u}) = \int_{\Omega} \nabla^s \mathbf{w} : C : \nabla^s \mathbf{u} \tag{3.69}$$

$$(\nabla \cdot \mathbf{w}, p)_{\Omega} = -\int_{\Omega} p \nabla \cdot \mathbf{w} d\Omega \tag{3.70}$$

$$(q, \nabla \cdot \mathbf{u} + p/\kappa)_{\Omega} = \int_{\Omega} q(\nabla \cdot \mathbf{u} + p/\kappa) d\Omega \tag{3.71}$$

$$(\mathbf{w}, \mathbf{f})_{\Omega} = \int_{\Omega} \mathbf{w} \cdot \mathbf{f} d\Omega \tag{3.72}$$

$$(\mathbf{w}, \mathbf{t})_{\partial\Omega_N} = \int_{\partial\Omega_N} \mathbf{w} \cdot \mathbf{t} d\Omega \tag{3.73}$$

3.6.2 Galerkin formulation and matrix problem

The Galerkin's counterpart of the weak formulation can be given as Find $\mathbf{u}_{hp} \in \mathbf{V}_{hp}$ and $p_{hp-1} \in Z_{hp-1}$ such that $\forall\ \mathbf{w}_{hp} \in \mathbf{W}_{hp}$ and $q_{hp-1} \in Z_{hp-1}$

$$d(\mathbf{u}_{hp}, \mathbf{w}_{hp}) - (\nabla \cdot \mathbf{w}_{hp}, p_{hp})_\Omega = (\mathbf{w}_{hp}, \mathbf{f})_\Omega + (\mathbf{w}_{hp}, \mathbf{t})_{\partial\Omega_N} \tag{3.74}$$

and

$$-(q_{hp-1}, \nabla \cdot \mathbf{u}_{hp} + p_{hp-1}/\kappa)_\Omega = 0 \tag{3.75}$$

where $\mathbf{V}_{hp} \subset \mathbf{V}$ and $\mathbf{W}_{hp} \subset \mathbf{W}$ and $Z_{hp-1} \subset Z$. Following the finite element method,

$$\mathbf{u}_{hp} = \sum_{i=1}^{M} N_i(x, y)\mathbf{u}_i \tag{3.76}$$

$$p_{hp-1} = \sum_{i=1}^{N} \widetilde{N}_i(x, y)p_i \tag{3.77}$$

and the weighting functions are chosen as the shape functions. Substitution of the expansion into the Galerkin formulation leads to the matrix equations in partitioned form, and solutions can be obtained for both velocities and pressure. The global matrix equation looks like

$$\begin{pmatrix} K_c & K_{up} \\ K_{pu} & K_{pp} \end{pmatrix} \begin{pmatrix} u \\ p \end{pmatrix} = \begin{pmatrix} R \\ 0 \end{pmatrix} \tag{3.78}$$

Each block component of the global stiffness matrix is shown below

$$K_c = \bigwedge_{e=1}^{E} {k_c}^{(e),ab} \tag{3.79}$$

$$K_{up} = \bigwedge_{e=1}^{E} {k_{up}}^{(e),ab} \tag{3.80}$$

$$K_{pu} = \bigwedge_{e=1}^{E} {k_{pu}}^{(e),ab} \tag{3.81}$$

$$K_{pp} = \bigwedge_{e=1}^{E} {k_{pp}}^{(e),ab} \tag{3.82}$$

Each elemental matrices are defined one by one as follows

$$k_c{}^{(e),ab} = \int_{\Omega^e} B^{a^T} \overline{D} B^b d\Omega \tag{3.83}$$

where $\overline{D}$ is defined as

$$\overline{D} = \mu \begin{pmatrix} 2 & 0 & 0 \\ 0 & 2 & 0 \\ 0 & 0 & 1 \end{pmatrix} \tag{3.84}$$

and the rest of the element matrices are

$$k_{up_e} = -\int_{\Omega^e} (\nabla N^a) \widetilde{N}^b d\Omega \tag{3.85}$$

$$k_{pu_e} = -\int_{\Omega^e} \widetilde{N}^a (\nabla N^b)^T d\Omega \tag{3.86}$$

$$k_{pp_e} = -\int_{\Omega^e} \widetilde{N}^a \widetilde{N}^b d\Omega \tag{3.87}$$

The *hp* discretization is used and relevant basis functions used are the same as before. Furthermore, the order of interpolation for the pressure is one order less than the velocity. From this point in this chapter, the following notations are used

A = Penalty function formulation

B = Mixed approach for penalty formulation

In order to differentiate the two approaches which were used for simulation, the conditioning of the element stiffness matrix is analyzed for increasing polynomial order for an optimal choice of Poisson's ratio of 0.4999999. The observation this time is by the way of calculating the eigenspectrum of the element stiffness matrix and plotting it in the real and imaginary plane. It is shown in Figure. 3.2. The discretization is for quadrilaterals and the formulation used for this plot is method **A**. It can be noticed that the eigenvalues always lie at the origin or in the positive side of the real line, which means that the matrix is always positive semi definite. Moreover, when the order is increased, the width of the eigenspectrum remains same. However, one must notice that, the order of the eigenvalues is found to be 10^7.

Another observation is that, as the order is increased, the number of eigenvalues clustered near zero increases. The matrix is singular as boundary conditions have not yet been imposed.

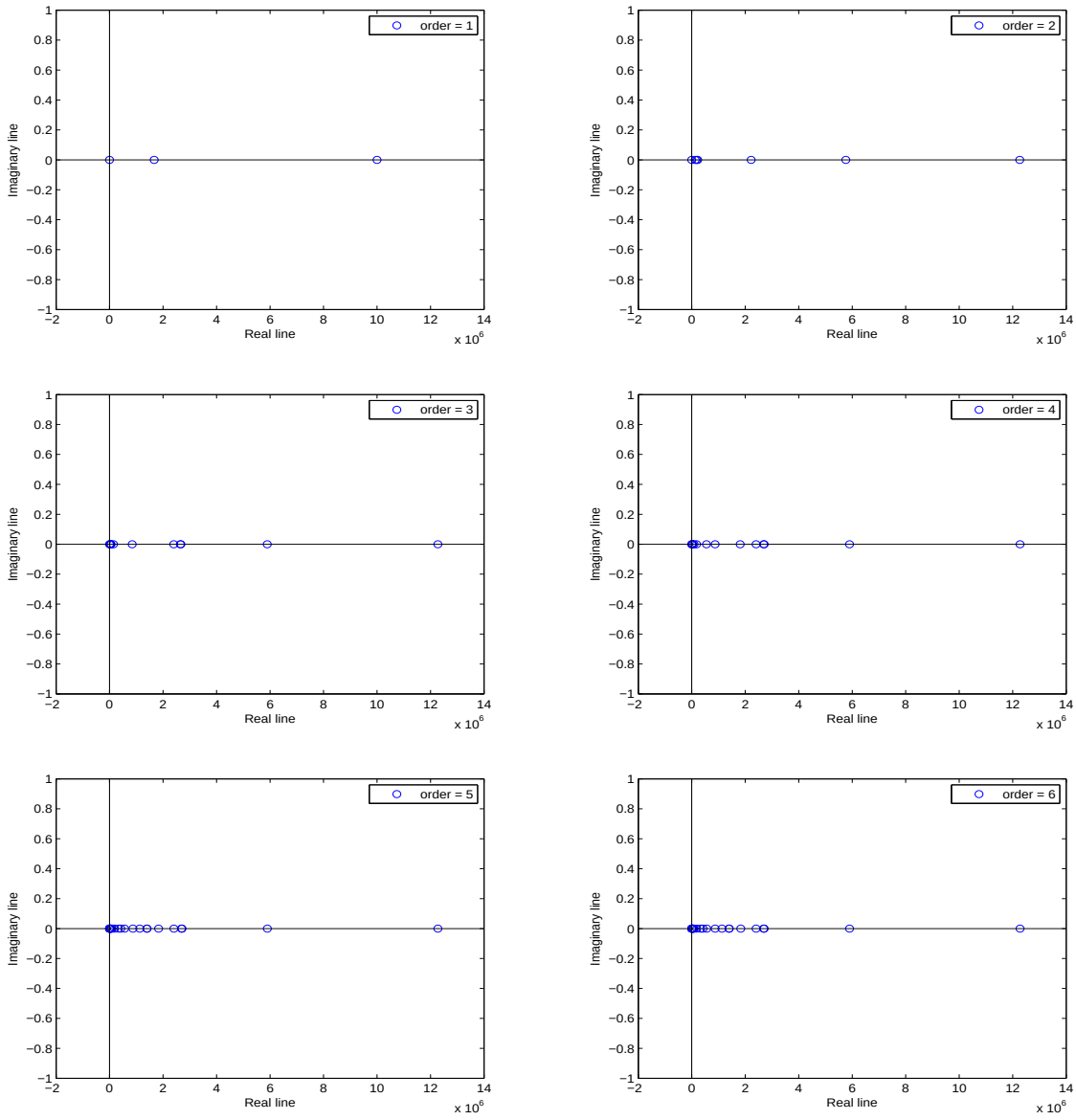

Figure 3.2: Eigenvalues from the element stiffness matrix for different orders-mixed method

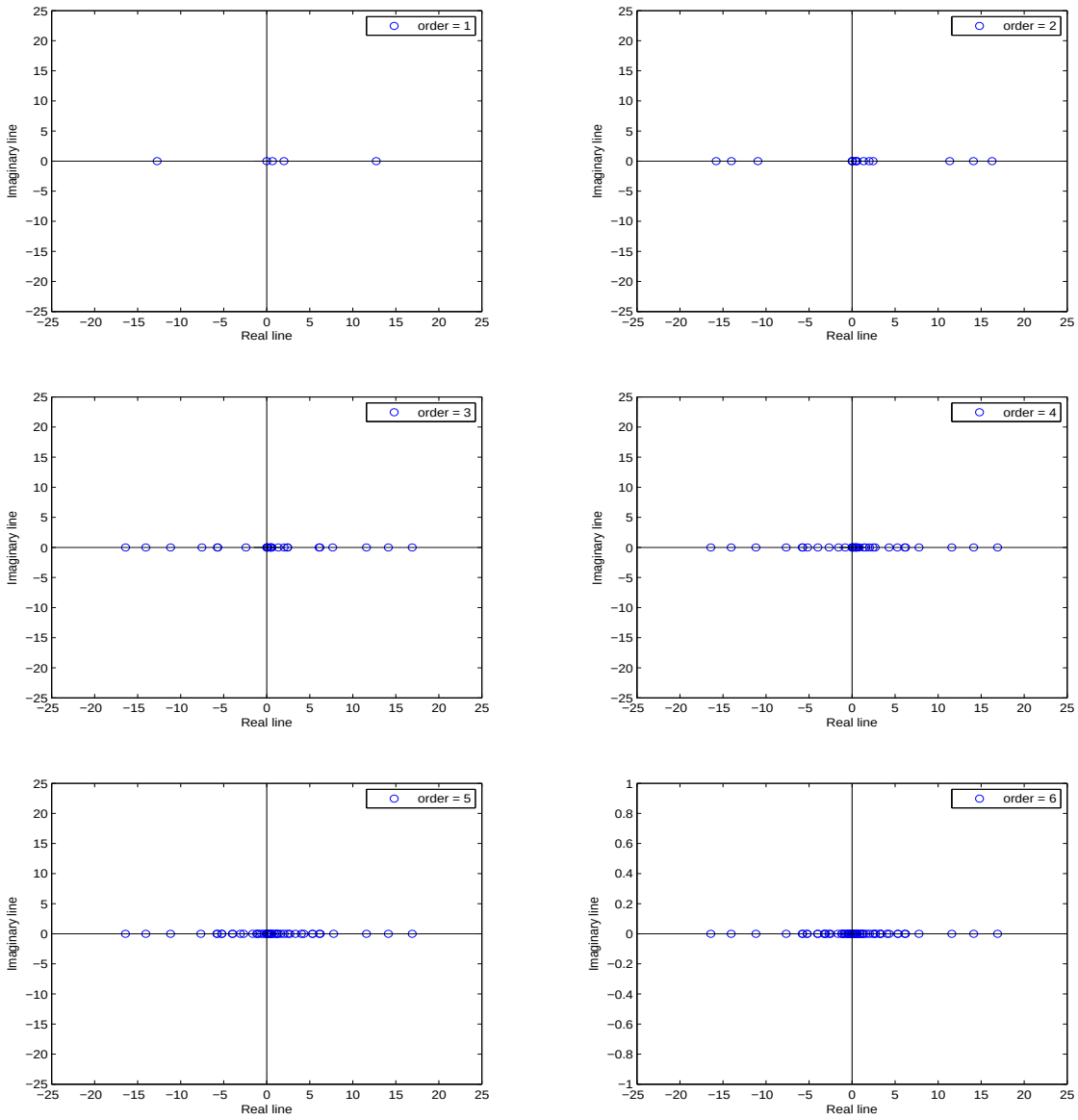

Figure 3.3: Eigenvalues from the element stiffness matrix for different orders-penalty function method

A similar plot is shown in Figure. 3.3 for method **B** using the same Poisson's ratio of 0.4999999 and a quadrilateral discretization. It can be seen that the eigenvalues are on both sides of the real line, implying that the matrix is indefinite. One can again notice that the width of the eigenspectrum remains approximately constant as the order increases, but there are increasing number of eigenvalues clustered around

zero. However, the major observation would be that, the value of the eigenvalues in the case of the method **A** is of the order 10^7, whereas the eigenvalues found in the method **B** is only 10^1. This means that the conditioning of the stiffness matrix in the method **B** is much better than the method **A**. So the method **B** alleviates the ill-conditioning of the stiffness matrix occurring in the method **A**.

3.7 Benchmark examples

Three benchmark problems are considered. The first two have analytical solutions and the final problem is benchmarked against reference solutions given in the literature. The first considers Poiseiulle's flow through a duct, which is a simplification of the Stokes flow problem. The second is a flow inside a square cavity and it has a forcing term on the right hand side of the Stokes equations, which induces a swirling flow inside the cavity. The third benchmark problem is the lid driven cavity problem which is a major example for validation of most of the existing Computational Fluid Dynamics (CFD) solvers. It does not have an analytical solution, but many numerical results are available in the literature which permit comparisons to be made. The first two problems which have analytical solutions are described as follows.

3.7.1 Poiseiulle's flow through a duct

For this benchmark problem, a rectangular duct is taken for analysis as shown in Figure. 3.4. The upper and the lower surfaces are the walls and flow moves from left to right.

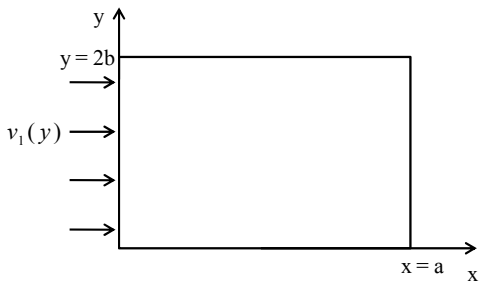

Figure 3.4: Poiseiulle's flow problem

The momentum equation for Stokes flow is

$$-\mu\nabla^2\mathbf{v} + \nabla p = \mathbf{f} \quad in \quad \Omega \tag{3.88}$$

In the the Poiseiulle's flow case, the velocities components in the x and y directions, v_1 and v_2 respectively, and the pressure satisfy the following relationships

$$v_2 = 0 \tag{3.89}$$

$$\frac{\partial v_1}{\partial x} = 0 \tag{3.90}$$

$$\frac{\partial p}{\partial y} = 0 \tag{3.91}$$

$$p = p(x) \tag{3.92}$$

Therefore eq. (3.88) simplifies to

$$\mu\frac{\partial^2 v_1}{\partial y^2} - \frac{\partial p}{\partial y} = 0 \tag{3.93}$$

Substituting $\dfrac{\partial p}{\partial x} = k$, a constant, implies

$$\mu\frac{\partial^2 v_1}{\partial y^2} = k \tag{3.94}$$

but it is known that $v_1 = f(y)$ and therefore the partial derivative can be replaced with a standard derivative. Using the notation $\dfrac{\partial^2 v_1}{\partial y^2} = \dfrac{d^2 v_1}{dy^2}$,

$$\frac{d^2 v_1}{dy^2} = \frac{k}{\mu} \tag{3.95}$$

In order to obtain the analytical solution, the above equation is integrated twice which implies

$$v_1(y) = \frac{k}{2\mu}y^2 + C_1 y + C_2 \tag{3.96}$$

where C_1 and C_2 are constants of integration. Now the no slip boundary conditions are applied, $v_1(0) = 0$ and $v_1(2b) = 0$, which implies $C_1 = \dfrac{kb}{\mu}$ and $C_2 = 0$. Therefore the analytical solution for this problem is

$$v_1 = \frac{k}{\mu}y\left(\frac{y}{2} - b\right) \tag{3.97}$$

3.7.2 Stokes flow with a prescribed body force

The problem at hand is the square domain shown in Fig. 3.5.

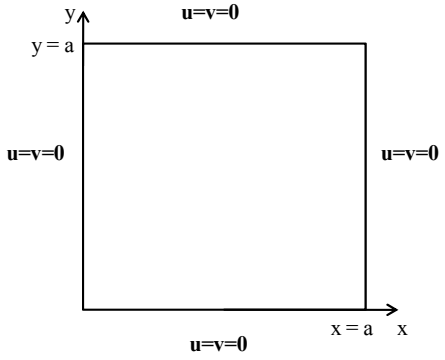

Figure 3.5: Problem domain

If the components of the body force are prescribed as

$$b_1 = (12-24y)x^4 + (-24+48y)x^3 + (-48y+72y^2-48y^3+12)x^2 \\ +(-2+24y-72y^2+48y^3)x + 1 - 4y + 12y^2 - 8y^3 \tag{3.98}$$

$$b_2 = (8-48y+48y^2)x^3 + (-12+72y-72y^2)x^2 + (4-24y+48y^2- \\ 48y^3+24y^4)x - 12y^2 + 24y^3 - 12y^4 \tag{3.99}$$

Then the stationary Stokes problem has a closed-form analytical solution [2]. For $\mu = 1$ [2] the exact solution for this problem is

$$v_1(x,y) = x^2(1-x)^2(2y-6y^2+4y^3) \tag{3.100}$$

$$v_2(x,y) = -y^2(1-y)^2(2x-6x^2+4x^3) \tag{3.101}$$

$$p(x,y) = x(1-x) \tag{3.102}$$

3.7.3 Lid driven cavity problem

The lid driven cavity problem with the boundary conditions is shown in Figure. 3.6.

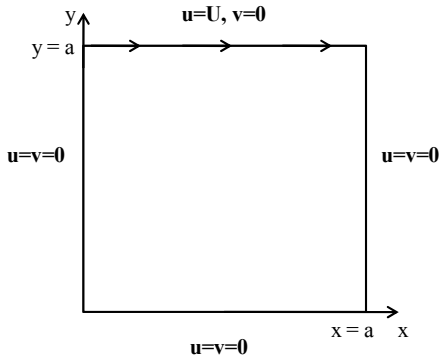

Figure 3.6: Lid driven cavity problem domain

The movement of the lid creates a low pressure zone inside the cavity and it causes the flow to develop circulation zones. It does not have any analytical solution, hence the results are to be compared with the available literature. The numerical results for all the benchmark problems described above will be discussed in the next section.

3.8 Numerical results and discussion

In this section the numerical results for the benchmark examples are shown and are compared with the benchmark solutions. The domain is discretized into a set of non-overlapping generic elements. Both quadrilaterals and triangles are used. Uniform meshes are considered for all the benchmark problems. A convergence analysis is done for both the formulations and for both discretizations, i.e. triangles and quadrilaterals. In order to show the accuracy of the results, the error has to be measured. Thus in the case of problems with analytical solution, the L_2 norm of the error is used, which is shown in the appendix. The convergence analysis is done for both the velocity and the pressure variables. The benchmark results are described in order of the problems presented in the previous section.

3.8.1 Results for Poiseiulle's flow through a duct

The first problem considered is the Poiseiulle's flow through a duct. The viscosity is chosen to be 100. The result is for a penalty function formulation with a quadrilateral mesh and uniform mesh spacing size function $h = 0.2$ and with quadratic order. The contour plot for the horizontal component of velocity is shown in the left in Figure. 3.7. The computed pressure is shown in the right in Figure. 3.7. Both profiles are behaving as expected. The result shown is convincing as it is conforming with the actual physics since the analytical solution is also of quadratic order. Figure. 3.8 shows a vector plot of the horizontal component of the velocity. It is observed to be parabolic as expected.

Next the convergence analysis is done for both methods **A** and **B** for the velocities. The value of ν is taken to be 0.4999999. First the convergence is shown for the method **A** for h and p refinements, and h refinements are for various orders $p = 1,\ 2,\ 3$ and 4, and p refinement is for various mesh spacings $h = 0.05,\ 0.1,\ 0.2$ and 0.3. The results for penalty function method are shown in Figure. 3.9 and Figure. 3.10. These figures show convergence of the error on a logarithmic scale for both triangles (left) and quadrilaterals (right). One can observe that there is no convergence in the case of h refinement for the first order with triangles as the locking occurs, but as the order is increased 2, the error drops to 10^{-7}, however there is no further drop in error with further h refinement since the analytical solution is also quadratic.

Next the convergence for method **B** for h and p refinements are shown in Figure. 3.11 and in Figure. 3.12. It can be observed for h refinement, that for the 1st order the convergence is not appreciable, and it is seen, that as the order increases, further h refinements are seen to be lying along a same line. Once again this is due to the fact that the analytical solution is quadratic. For the p convergence it is seen that the convergence is exponential, upto order 2 and then it stagnates on the same line. The trend is the same for all mesh spacings as shown in the figure. Thus it can be ascertained that the results are conforming well with the analytical solution. Furthermore the locking phenomenon does not occur for method **B** during

h refinements in both triangles and quadrilaterals. All p refinements show that, with second order elements and above, the solution is optimal. The maximum error achieved for both methods **A** and **B** is dictated by the choice of the value of the Poisson's ratio ν, the effect of which will be shown soon.

The profile of velocity is obtained at the vertical center of the duct is shown in Figure. 3.13. It is seen that for order $p = 2$ and $h = 0.2$ the resulting velocity profile exactly matches with the analytical solution.

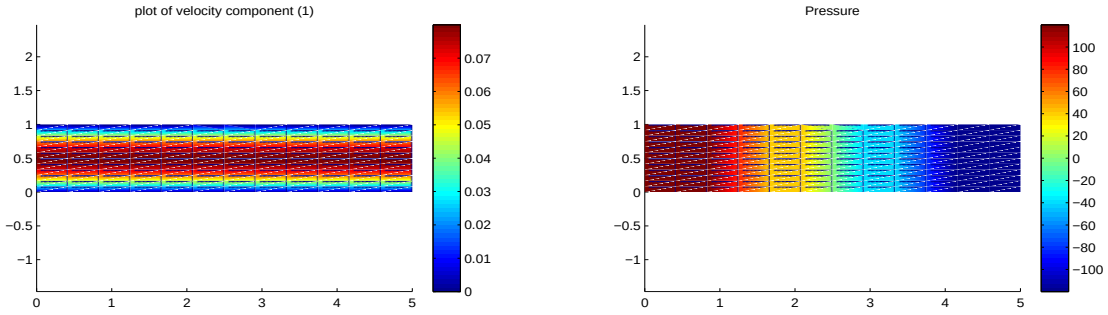

Figure 3.7: Velocity and pressure contours

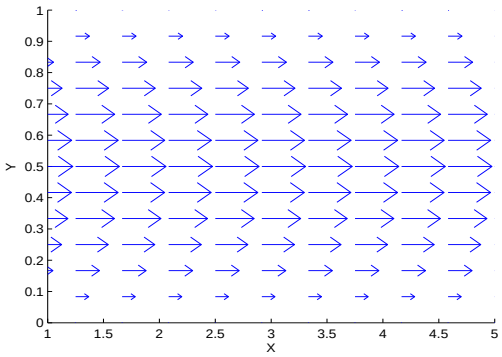

Figure 3.8: Horizontal velocity vector plot

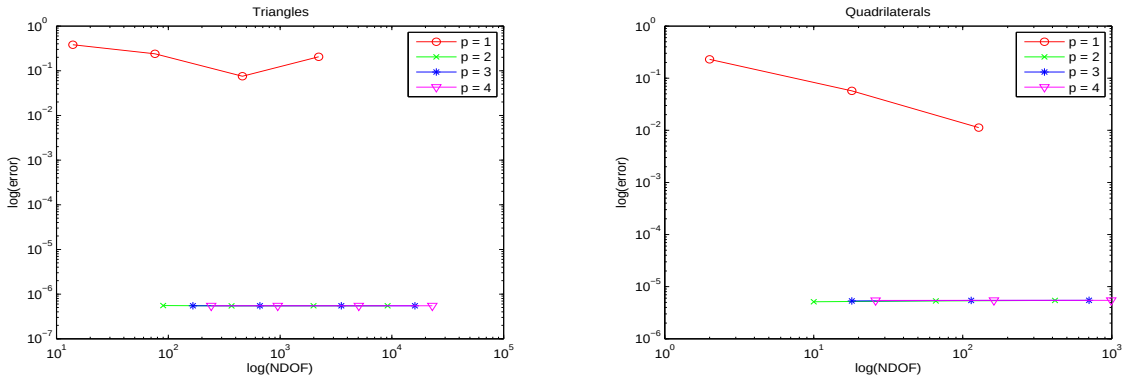

Figure 3.9: h convergence for triangles and quadrilaterals in method **A** for velocity

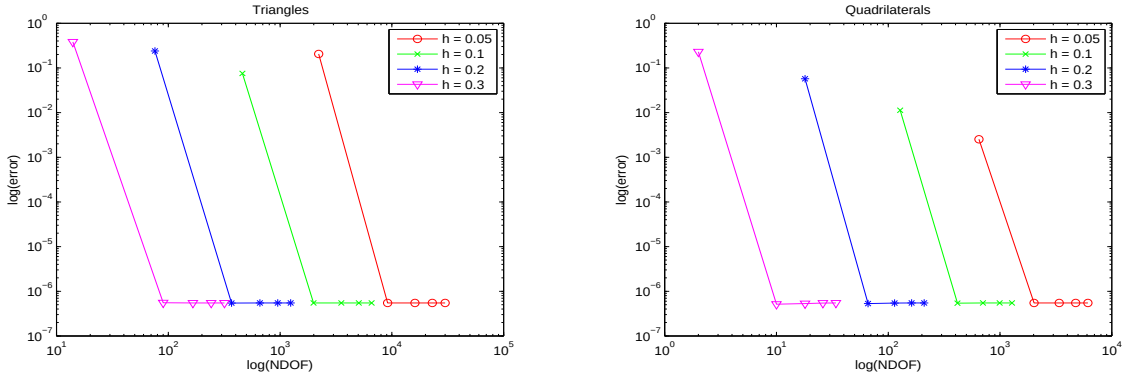

Figure 3.10: p convergence for triangles and quadrilaterals in method **A** for velocity

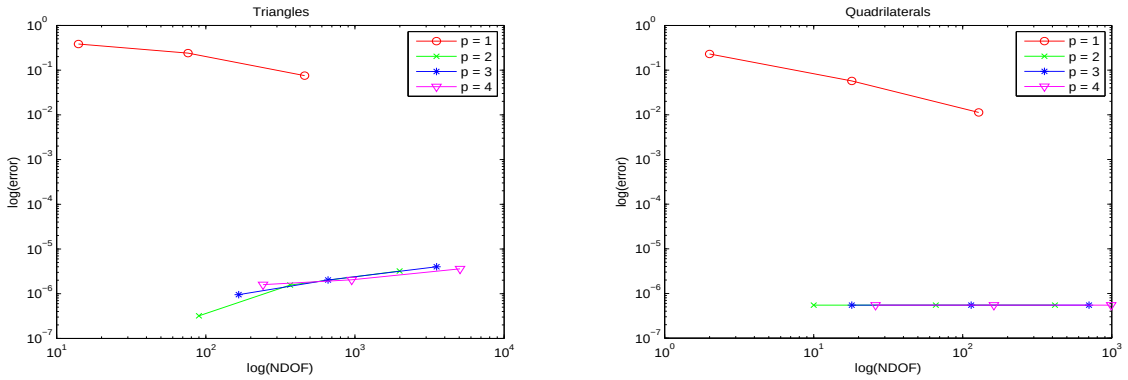

Figure 3.11: h convergence for triangles and quadrilaterals in method **B** for velocity

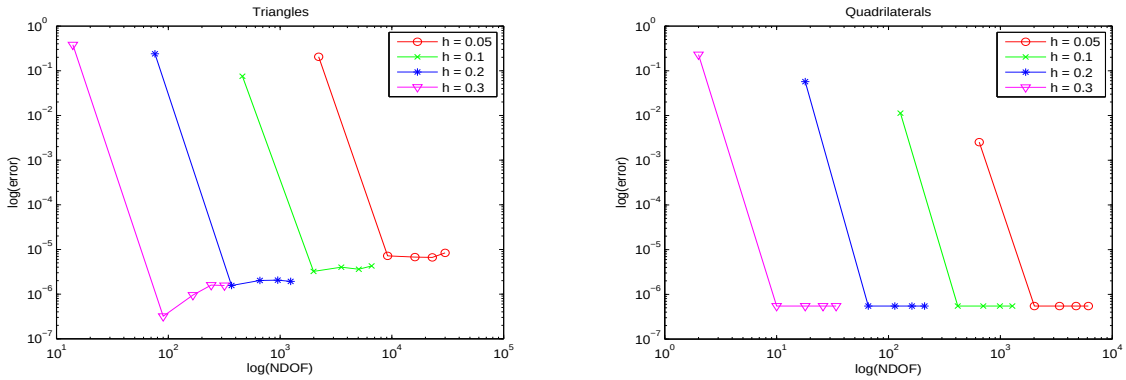

Figure 3.12: p convergence for triangles and quadrilaterals in method **B** for velocity

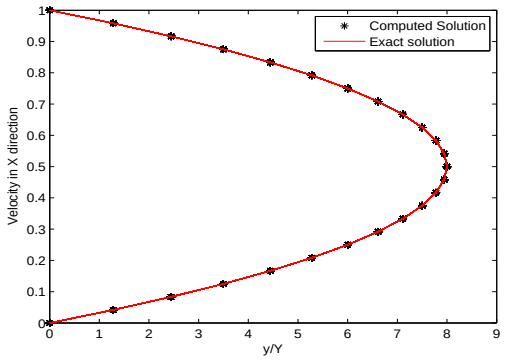

Figure 3.13: Comparison of horizontal velocity profile with exact solution

3.8.2 Results for Stokes flow with a prescribed body force

Next the numerical results for benchmark problem of the Stokes flow with prescribed body force is analyzed. The contour plot of the horizontal velocity is shown in Figure. 3.14. The countour plot is shown for method **B** for triangles with order 4 and with mesh spacing h as 0.1 The velocity vector plot for the same is given in Figure. 3.15. It is seen that there is a low pressure region created at the geometric center and a symmetric swirling flow pattern is observed. Next the pressure contour for the same mesh is shown in Figure. 3.16. It matches very well with exact solution obtained in [2] and is shown in Figure. 3.17.

Now the convergence analysis for velocity is done for this problem. First the convergence results for the method **A** are described in Figure. 3.18 and in Figure. 3.19. It can be observed that for h refinement using both triangular and quadrilateral meshes, that the convergence is algebraic, and locking is observed for the 1st order elements in quadrilaterals. One will also observe that, the error w.r.t h refinement for quadrilateral mesh with order 4 is already at the optimum value because of the choice of ν. Further h refinement leads to increase in the error due to the ill-conditioning of the system matrix. With p refinement, exponential convergence is obtained.

Next the results of method **B** are shown in Figure. 3.20 and in Figure. 3.21. Both the convergence for triangles and quadrilaterals are shown in these figures. It can be observed that the p convergence for the quadrilaterals, for all the meshes stagnates at order 4 but for triangles it requires order 7. The reason being that, due to the tensor product structure of the problem and since quadrilaterals are already bilinear in nature at the lowest order case and that for higher order, the quadrilaterals are able to reproduce solution of the form $f(x)f(y)$ with both $f(x)$ and $f(y)$ of degree p, the accurately capture the solution at the order 4. In the case of triangles, which don't have a tensor product structure, they capture the solution only with elements of order 7 or more. Apart from the above discussion, the other observation is that the p convergence for different mesh spacings are exponential for both triangles and quadrilaterals. The h convergence is algebraic.

Next the variation in L_2 norm of numerical error in velocity solution is studied for various values of the Poisson's ratio, keeping other parameters constant. The method **B** is used and the discretization consists of a mesh of uniformly sized triangles with spacing $h = 0.1$ and order $p = 4$. The Figure. 3.26 shows the Poisson's ratio vs the error, with error in logarithmic scale. It can be inferred that, as the Poisson's ratio goes closer to 0.5, the error drops down steeply, and this requires further magnification of the region representing the Poisson's ration very near to 0.5. The zoomed region is shown in Figure. 3.27. The plot now is in logarithmic scale in Poisson's ratio and the error to capture the change in the plot effectively. It can be observed that the error

decreases to some point close to 0.5 and then increases. The reason for the increase in error is due to the ill-conditioning associated with the choice of ν very close to 0.5. In the limiting case of $\nu = 0.5$, the matrix is singular. The optimal value of the Poisson's ratio found from this plot is employed for all the simulations.

The convergence analysis for pressure is subsequently shown for methods **A** and **B**. From figure. 3.22 it is observed that h convergence for triangles is algebraic and is very slow and at the maximum only one order reduction in magnitude can be seen, whereas there is no h convergence for quadrilaterals. The Figure. 3.23 shows the p convergence for the method **A**. For the triangles there is only a one order of magnitude fall, whereas for quadrilaterals there is a two order of magnitude fall, but for both the discretizations, the the convergence does not go down beyond 10^{-2}, as the order p is increased. Next the h convergence for method **B** is shown in Figure. 3.24. For both triangles and quadrilaterals, the convergence is algebraic and it there is one order of magnitude fall. But it is better than the method **A** for the quadrilaterals since, in the method **A**, there was no h convergence for quadrilaterals. Next the Figure. 3.25 shows the p convergence for pressure in the method **B**. It can be seen for triangles that the convergence is not rapid and it stops around 10^{-1}, which is not good, and is similar to the method **A**. However, the p convergence for quadrilaterals is better than the method **A**, as it can be observed that for the mesh spacing 0.05, there is 3 order fall upto 10^{-3}. Furthermore the convergence for the pressure is not very satisfactory since, it is not the the hydrostatic pressure, i.e. the incompressible constraint is not strictly imposed.

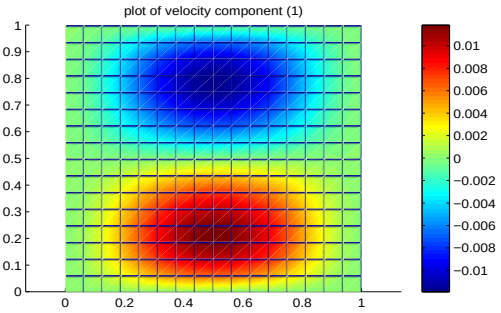

Figure 3.14: Horizontal velocity contour

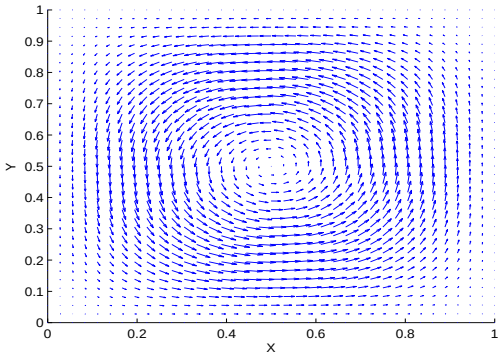

Figure 3.15: Horizontal velocity vector plot

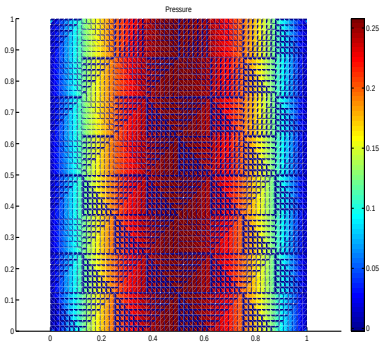

Figure 3.16: Pressure plot in the domain

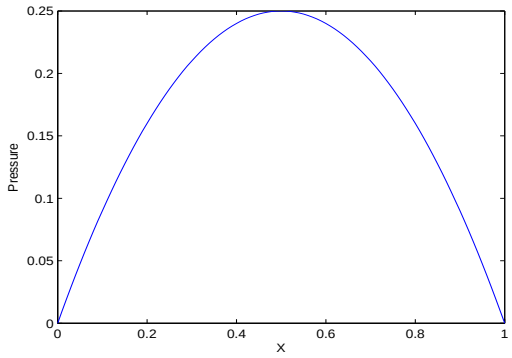

Figure 3.17: Pressure plot in the domain (exact) as in [2]

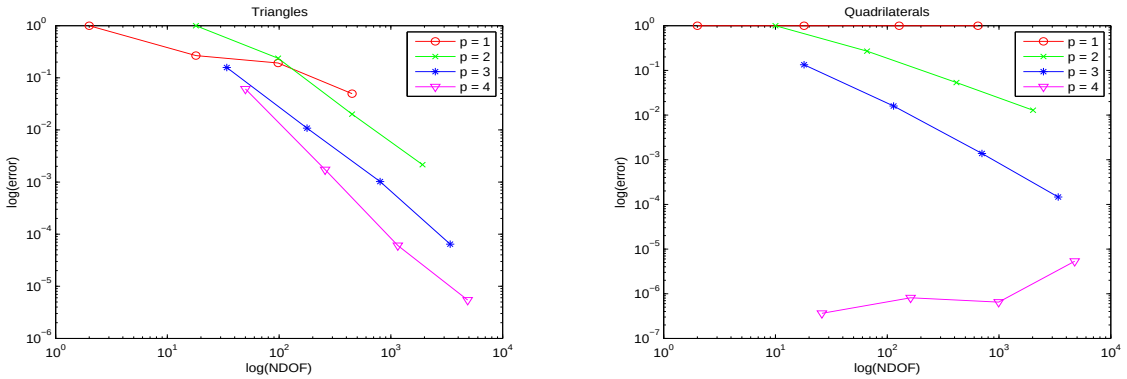

Figure 3.18: h convergence for triangles and quadrilaterals in method **A** for velocity

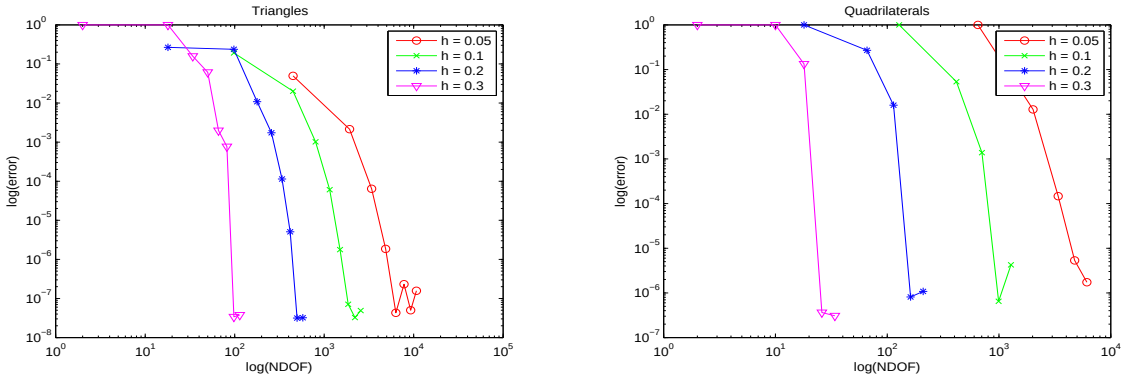

Figure 3.19: p convergence for triangles and quadrilaterals in method **A** for velocity

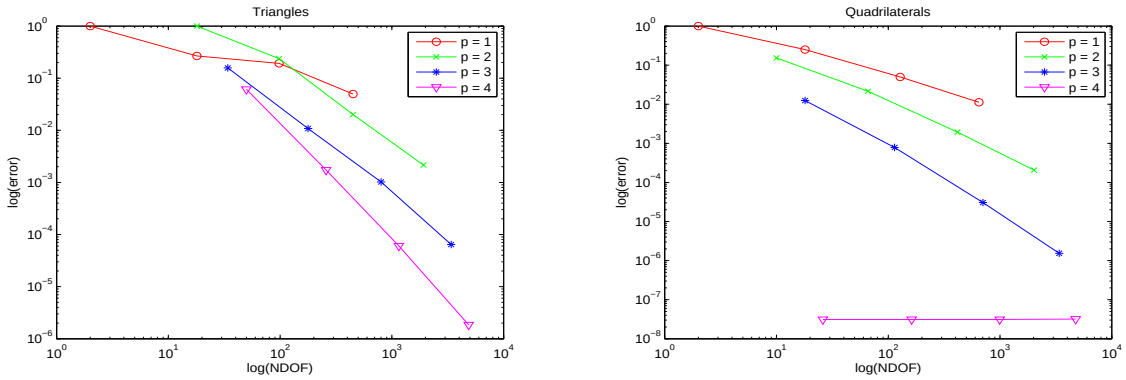

Figure 3.20: h convergence for triangles and quadrilaterals in method **B** for velocity

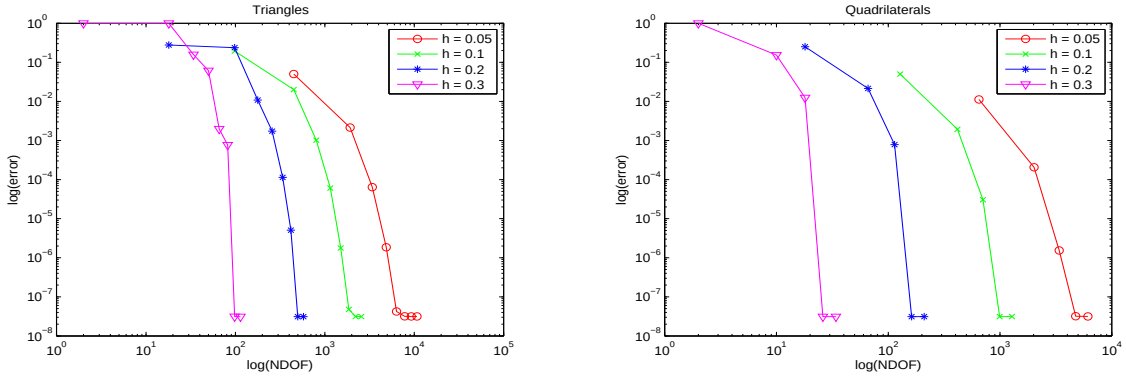

Figure 3.21: p convergence for triangles and quadrilaterals in method **B** for velocity

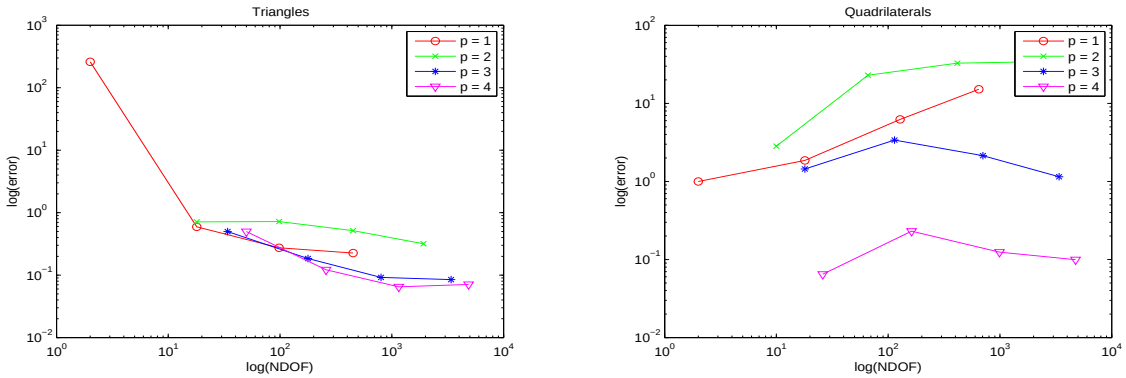

Figure 3.22: h convergence for triangles and quadrilaterals in method **A** for pressure

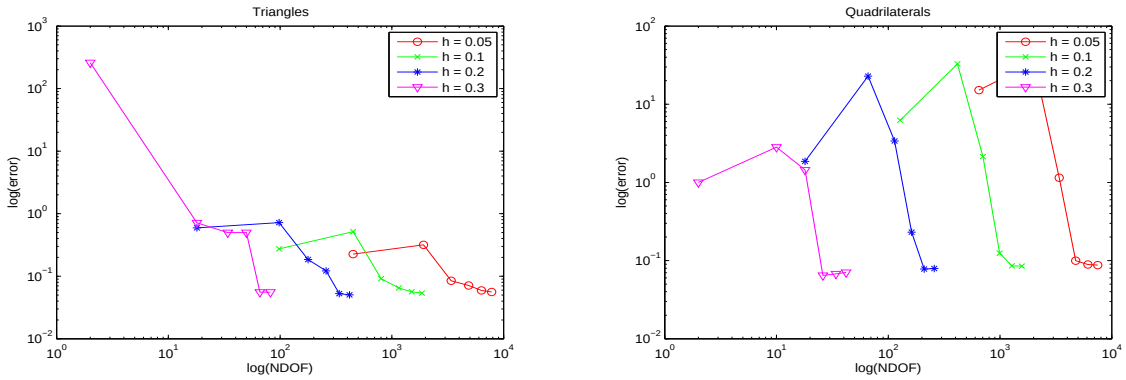

Figure 3.23: p convergence for triangles and quadrilaterals in method **A** for pressure

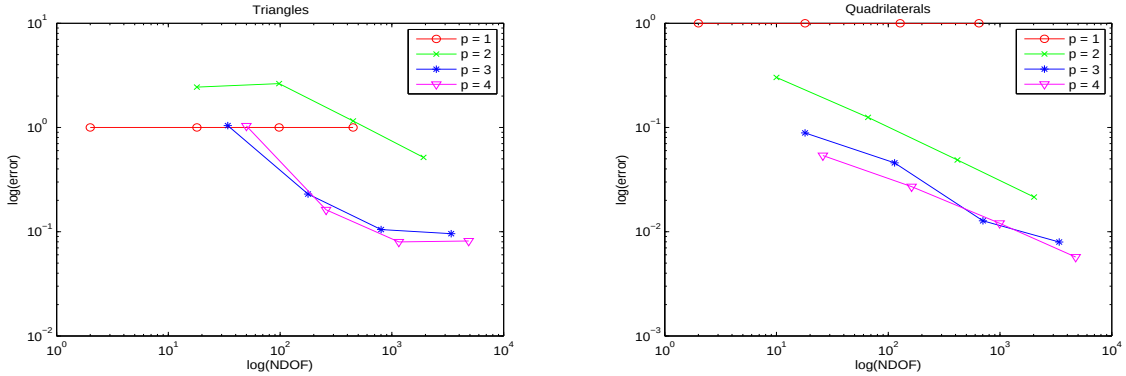

Figure 3.24: h convergence for triangles and quadrilaterals in method **B** for pressure

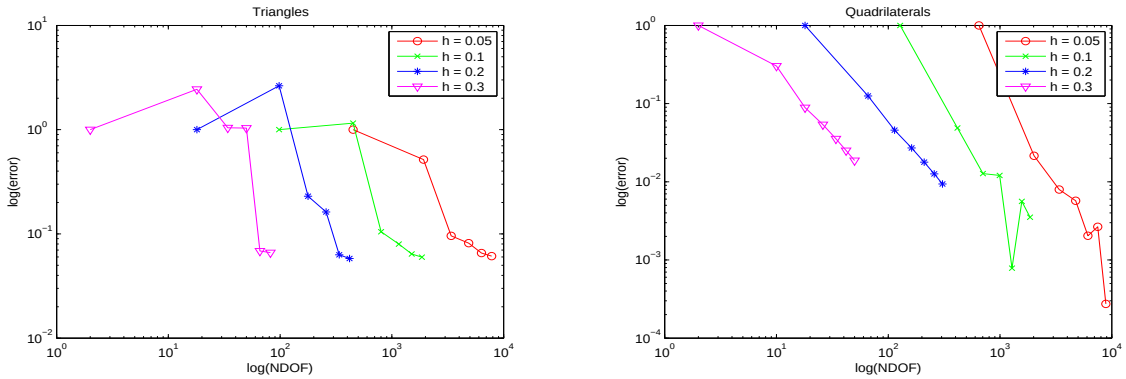

Figure 3.25: p convergence for triangles and quadrilaterals in method **B** for pressure

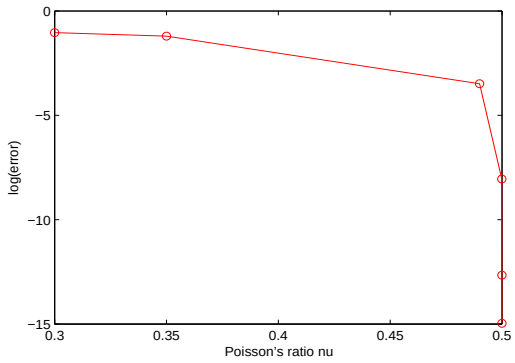

Figure 3.26: Logarithm of error vs the logarithm of $(\nu - 0.5)$

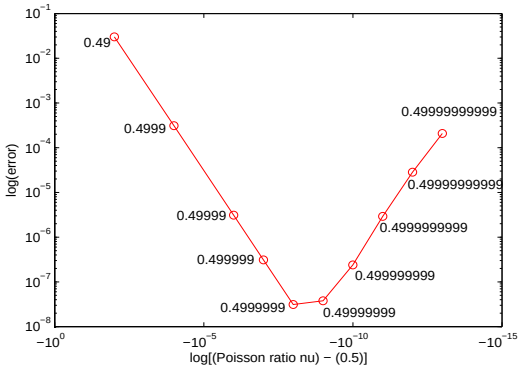

Figure 3.27: Logarithm of error vs the logarithm of $(\nu - 0.5)$ [zoomed]

3.8.3 Results for lid driven cavity problem

Now the numerical results of benchmark problem of Lid driven cavity is analyzed. The method **B** is used with a triangular mesh. Since this problem does not posses an analytical solution, the established benchmark numerical results in the literature are used to compare with the computed solution. First the contour plot of the horizontal velocity is shown in Figure. 3.28. If looked closely, it can be observed that there is a primary vortex formed at the center. It can be clearly seen in the vector plot in Figure. 3.29. Next the Figure. 3.30, the computed profile of horizontal velocity along the vertical geometric center is compared with the literature [2]. The numerical result

matches exactly with the literature profile [2]. Next the result is compared with the other standard references in the literature in Figure. 3.31. Although the numerical result is compared directly with the Navier Stokes solutions given in the literature, it is to be noted that as the Reynolds number decreases the computed velocity profile coincides more with the profile in the literature. Furthermore, the same velocity profile is computed for increasing order and compared with the reference. It is shown in Figure. 3.32. It can be noted in this figure that, as the order increases, the numerically computed velocity profile matches well with the literature profile [2].

Thus the results are discussed in detail for the validation of the solver with the benchmark problems. Nice convergence of all the problems considered shows that the code has been successfully benchmarked.

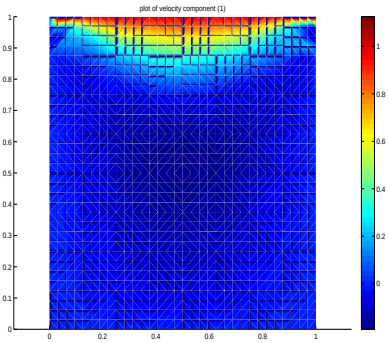

Figure 3.28: Contour plot for the horizontal velocity

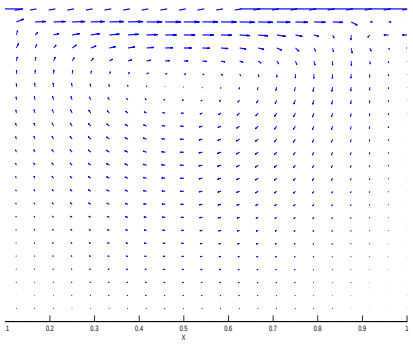

Figure 3.29: Vector plot for the horizontal velocity

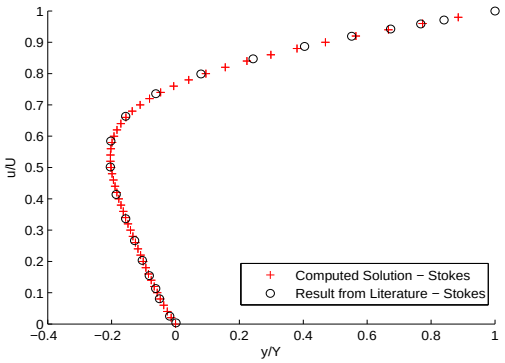

Figure 3.30: Horizontal velocity profile along the vertical center line in the domain - comparison with Stokes solution in [2]

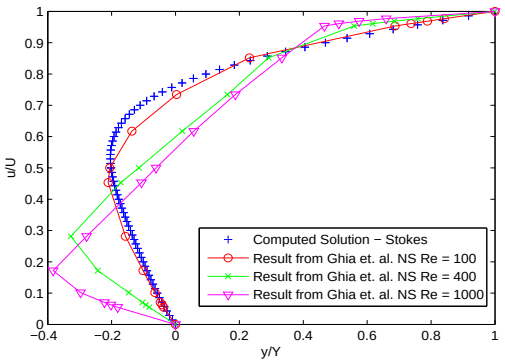

Figure 3.31: Horizontal velocity profile along the vertical center line in the domain - comparison with Navier Stokes solution in [3]

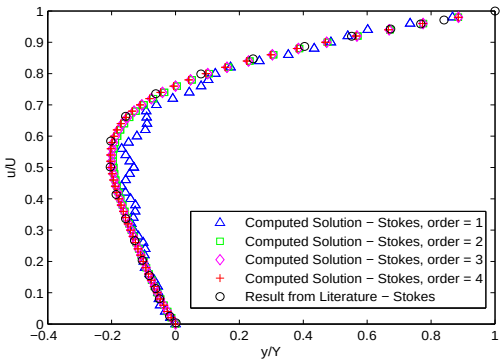

Figure 3.32: Convergence of the velocity with increase in order

Chapter 4

Analysis of the coupled problem

4.1 Introduction

Chapter 2 and chapter 3 involve the analysis of the individual fields of electrostatics and fluid mechanics. In this chapter, the coupled problem of electrostrictive fluids is treated, where the electrostatics field and fluid mechanical field is coupled, the fluid being a dielectric. Initially the equations governing electrostatics and fluid mechanics are once again introduced. Next the equations governing the coupled problem is presented and the finite element formulation is described. The algorithm for the coupled solution is presented next and finally a series of numerical examples are presented and simulation results are shown.

4.2 Governing equations of electrostatics and fluid mechanics

As a precursor to this chapter, a reminder of the governing equation of electrostatics and fluid mechanics are presented. The strong form of electrostatics problem is shown below

$$\begin{aligned} \nabla \cdot (\epsilon_r \nabla \phi) &= 0 \quad \text{in} \quad \Omega_E \\ \phi &= \phi_D \quad \text{on} \quad \partial\Omega_E^D \\ \mathbf{n} \cdot (\epsilon_r \nabla \phi) &= f_N \quad \text{on} \quad \partial\Omega_E^D \end{aligned} \tag{4.1}$$

where ϕ is the electrostatic potential, ϵ_r is the relative permittivity, Ω_E is the electrostatic domain, $\partial\Omega_E^D$ is the Dirichlet boundary and $\partial\Omega_E^N$ is the Neumann boundary in the domain and the complete electrostatic boundary is $\partial\Omega_E = \partial\Omega_E^D \cup \partial\Omega_E^N$. Once

the ϕ is determined, the scaled electric field can be computed by $\mathbf{E} = -\nabla\phi$. Next the strong form of the fluid mechanics problem is shown below

$$\begin{aligned} -\mu\nabla^2\mathbf{u} + \nabla p &= \mathbf{f} && \text{in} \quad \Omega_F \\ \nabla \cdot \mathbf{u} &= 0 && \text{in} \quad \Omega_F \\ \mathbf{u} &= \mathbf{u}_D && \text{on} \quad \partial\Omega_F^D \\ \mathbf{t} &= -\mathbf{n}p + \mu(\mathbf{n}\cdot\nabla)\mathbf{u} && \text{on} \quad \partial\Omega_F^N \end{aligned} \tag{4.2}$$

where $\mathbf{u}$ is the velocity, p is the pressure, μ is the dynamic viscosity, $\mathbf{t}$ is the traction, $\mathbf{u}_D$ is the velocity at the Dirichlet boundary, Ω_F is the fluid mechanics domain, $\partial\Omega_F^D$ is the Dirichlet boundary and $\partial\Omega_F^N$ is the Neumann boundary in the domain and the complete fluid mechanical boundary is $\partial\Omega_F = \partial\Omega_F^D \cup \partial\Omega_F^N$.

4.3 The electrostrictive fluid problem

Electrostriction is an effect which arises when the domains of the electrostatics and fluid mechanics intersect, as it is shown in Fig. 4.1.

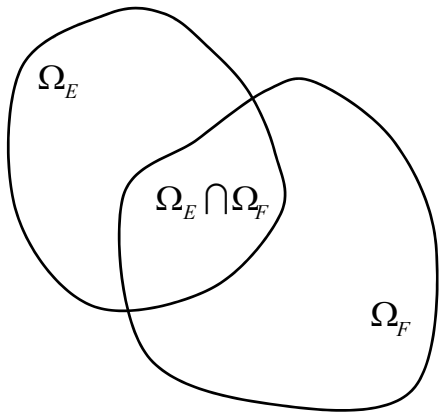

Figure 4.1: Problem domain for electrostriction

In the coupled problem $\Omega_E \cap \Omega_M \neq 0$. The term electrostriction comes from the property of the dielectric medium, which deforms under the application of an electric field. So, in the electrostrictive fluid problem, when the electric field is applied, there is a deformation in the fluid. This effect can be represented by a source term on the

right hand side of the momentum equation of the fluid, which can be written as

$$\tilde{\mathbf{f}} = \mathbf{f}_E + \mathbf{f} \tag{4.3}$$

where $\tilde{\mathbf{f}}$ is the total body force of the problem, which is a combination of the body force in the fluid mechanics domain, $\mathbf{f}$ and the body force due to the electrostrictive effect, $\mathbf{f}_E$. The electrostrictive body force is given as

$$\mathbf{f}_E = \nabla \cdot \sigma_E \tag{4.4}$$

where σ_E is the stress acting due to the electric field. In this particular case of an electrostrictive fluid, it can be expanded [20] as

$$\sigma_E = (\sigma_E)_0 + (\sigma_E)_F \tag{4.5}$$

The term $(\sigma_E)_0$ denotes the Maxwell stress and accounts for the effects associated to the existence of an electric field in free space and the term $(\sigma_E)_F$ is due to the existence of a dielectric material perturbing the free space [21]. The term $(\sigma_E)_0$ can be written as

$$(\sigma_E)_0 = \epsilon_0 \mathcal{E} \otimes \mathcal{E} - \frac{\epsilon_0}{2}(\mathcal{E} \cdot \mathcal{E})\mathbb{I} \tag{4.6}$$

where $\mathcal{E}$ is the electric field vector. The eq. (4.6) can also be re-written in terms of the rescaled electric field vector as

$$(\sigma_E)_0 = \mathbf{E} \otimes \mathbf{E} - \frac{1}{2}(\mathbf{E} \cdot \mathbf{E})\mathbb{I} \tag{4.7}$$

The other part $(\sigma_E)_F$ can be written as

$$(\sigma_E)_F = \epsilon_0(\epsilon_r - 1)\mathcal{E} \otimes \mathcal{E} - \frac{\epsilon_0}{2}(\epsilon_r - 1)(\mathcal{E} \cdot \mathcal{E})\mathbb{I} \tag{4.8}$$

which can be re-written interms of rescaled electric field as

$$(\sigma_E)_F = (\epsilon_r - 1)\mathbf{E} \otimes \mathbf{E} - \frac{1}{2}(\epsilon_r - 1)(\mathbf{E} \cdot \mathbf{E})\mathbb{I} \tag{4.9}$$

Therefore the electrostrictive stress σ_E in terms of the rescaled electric field becomes

$$\sigma_E = \epsilon_r \mathbf{E} \otimes \mathbf{E} - \frac{\epsilon_r}{2}(\mathbf{E} \cdot \mathbf{E})\mathbb{I} \tag{4.10}$$

This solution in eq. (4.10) is obtained by substituting dielectric constants $\epsilon_r^1 = 0$ and $\epsilon_r^2 = 0$ into the form of $(\sigma_E)_0$ and $(\sigma_E)_F$ for the general electrostrictive material as described by Gil and Ledger [21]. Next the strong form of the problem is shown.

4.3.1 Strong form of the problem and Galerkin formulation

Since a partitioned approach is used, one must first obtain the solution for the electrostatic problem and then solve the electrostrictive fluid problem. Hence the strong form of the electrostatics problem has to be defined first. It is defined once again as

$$\begin{aligned} \nabla \cdot (\epsilon_r \nabla \phi) &= 0 \quad \text{in} \quad \Omega_E \\ \phi &= \phi_D \quad \text{on} \quad \partial\Omega_E^D \\ \mathbf{n} \cdot (\epsilon \nabla \phi) &= f_N \quad \text{on} \quad \partial\Omega_E^D \end{aligned} \tag{4.11}$$

Next the strong form of the electrostrictive fluid problem can be stated as follows

$$\begin{aligned} -\mu\nabla^2\mathbf{u} + \nabla p &= \tilde{\mathbf{f}} && \text{in} \quad \Omega_F \\ \tilde{\mathbf{f}} &= \mathbf{f} && \text{in} \quad \Omega_F \setminus (\Omega_F \cap \Omega_E) \\ \tilde{\mathbf{f}} &= \mathbf{f} + \nabla \cdot \sigma_E && \text{in} \quad \Omega_F \cap \Omega_E \\ \sigma_E &= \epsilon_r \mathbf{E} \otimes \mathbf{E} - \tfrac{\epsilon_r}{2}(\mathbf{E} \cdot \mathbf{E})\mathbb{I} && \text{in} \quad \Omega_F \cap \Omega_E \\ \mathbf{u} &= \mathbf{u}_D && \text{on} \quad \partial\Omega_F^D \\ \tilde{\mathbf{t}} &= \mathbf{t} + \mathbf{n} \cdot \sigma_E && \text{on} \quad \partial\Omega_F^N \cap \partial(\Omega_F \cap \Omega_E) \\ \tilde{\mathbf{t}} &= \mathbf{t} && \text{on} \quad \partial\Omega_F^N \setminus (\partial\Omega_F^N \cap \partial(\Omega_F \cap \Omega_E)) \end{aligned} \tag{4.12}$$

where $\tilde{\mathbf{t}}$ is the traction vector which is equal to $\mathbf{t} + \mathbf{n} \cdot \sigma_E$ on the part of Neumann boundary for the fluid problem that intersects with the electrostatic domain and equal to t everywhere. Two different formulations discussed in the previous chapter are used for analysis, namely the penalty function formulation and the mixed approach for the penalty formulation, which would be called as mixed method in this chapter for convenience. Their respective weak forms are shown in the subsequent section.

4.3.2 Weak form of the problem

Initially the weak form of the electrostatic problem is defined. The trial and test spaces for the electric potential is given as

$$X = \{\phi \in (H^1(\Omega_E)), \phi = \phi_D \ \ on \ \ \partial\Omega_E^D\} \tag{4.13}$$

$$Y = \{\phi \in (H^1(\Omega_E)), \phi = 0 \ \ on \ \ \partial\Omega_E^D\} \tag{4.14}$$

$$\tag{4.15}$$

Hence the weak form can be stated as
find $\phi \in \ X$ such that

$$(\epsilon_r \nabla\phi, \nabla w)_{\Omega_E} = \int_{\partial\Omega_E^N} \mathbf{n} \cdot \epsilon_r \nabla\phi w d\Omega + (\rho_V, w)_{\Omega_E} \quad \forall w \in Y \tag{4.16}$$

where

$$(\epsilon_r \nabla\phi, \nabla w)_{\Omega_E} = \int_{\Omega_E} \epsilon_r \nabla\phi \cdot \nabla w d\Omega \tag{4.17}$$

$$(\rho_V, w)_{\Omega_E} = \int_{\Omega_E} \rho_v w d\Omega \tag{4.18}$$

Next the weak form for the electrostrictive fluid is written. The trial and test spaces for the velocity and the pressure are defined as

$$\mathbf{V} = \{\mathbf{u} \in (\boldsymbol{H}^1(\Omega_F)), \mathbf{u} = \mathbf{u}_D \ \ on \ \ \partial\Omega_F^D\} \tag{4.19}$$

$$\mathbf{W} = \{\mathbf{w} \in (\boldsymbol{H}^1(\Omega_F)), \mathbf{w} = \mathbf{0} \ \ on \ \ \partial\Omega_F^D\} \tag{4.20}$$

$$Z = \{p \in L^2(\Omega_F)\} \tag{4.21}$$

This weak form of the problem for the penalty and mixed method, follows in the same veins to the one shown in the previous chapter except that, this time there is the additional two components in the right hand side due to electrostriction. Hence, the weak form for the penalty function formulation can be written as
find $\mathbf{u} \in \mathbf{V}$ such that $\forall\ \mathbf{w} \in \mathbf{W}$

$$a(\mathbf{u}, \mathbf{w})_{\Omega_F} = (\mathbf{w}, \mathbf{f})_{\Omega_F} + (\mathbf{w}, \mathbf{t})_{\partial\Omega_F^N} + b(\sigma_E, \mathbf{w})_{\Omega_E \cap \Omega_F} + c(\sigma_E, \mathbf{w})_{\partial(\Omega_E \cap \Omega_F)} \tag{4.22}$$

where

$$a(\mathbf{u},\mathbf{w})_{\Omega_F} = \int_{\Omega_F} \nabla^s \mathbf{w} : C : \nabla^s \mathbf{u} \partial\Omega - \int_{\Omega_F} \lambda(\nabla\cdot\mathbf{u})(\nabla\cdot\mathbf{w}) d\Omega \quad (4.23)$$

$$(\mathbf{w},\mathbf{f})_{\Omega_F} = \int_{\Omega_F} \mathbf{w}\cdot\mathbf{f} d\Omega \quad (4.24)$$

$$(\mathbf{w},\mathbf{t})_{\partial\Omega_F^N} = \int_{\partial\Omega_F^N} \mathbf{w}\cdot\mathbf{t} d\Omega \quad (4.25)$$

$$b(\sigma_E,\mathbf{w})_{\Omega_E\cap\Omega_F} = \int_{\Omega_E\cap\Omega_F} \sigma_E : \nabla\mathbf{w} d\Omega \quad (4.26)$$

$$c(\sigma_E,\mathbf{w})_{\partial(\Omega_E\cap\Omega_F)} = \int_{\partial(\Omega_E\cap\Omega_F)} \mathbf{w}\cdot(\sigma_E\mathbf{n}) d\Omega \quad (4.27)$$

Similarly the weak form for the mixed method, where the solution is obtained for both velocities and pressure, can be written as

find $\mathbf{u}\in\mathbf{V}$ and $p\in Z$ such that $\forall\ \mathbf{w}\in\mathbf{W}$ and $q\in Z$

$$d(\mathbf{u},\mathbf{w})_{\Omega_F} - (\nabla\cdot\mathbf{w},p)_{\Omega_F} = (\mathbf{w},\mathbf{f})_{\Omega_F} + (\mathbf{w},\mathbf{t})_{\partial\Omega_F^N} + e(\sigma_E,\mathbf{w})_{\Omega_E\cap\Omega_F} + f(\sigma_E,\mathbf{w})_{\partial(\Omega_E\cap\Omega_F)} \quad (4.28)$$

$$-(q,\nabla\cdot\mathbf{u} + p/\kappa)_{\Omega_F} = 0 \quad (4.29)$$

where

$$d(\mathbf{u},\mathbf{w})_{\Omega_F} = \int_{\Omega_F} \nabla^s \mathbf{w} : C : \nabla^s \mathbf{u} \quad (4.30)$$

$$(\nabla\cdot\mathbf{w},p)_{\Omega_F} = \int_{\Omega_F} \lambda(\nabla\cdot\mathbf{u})(\nabla\cdot\mathbf{w}) d\Omega \quad (4.31)$$

$$(q,\nabla\cdot\mathbf{u}+p/\kappa)_{\Omega_F} = \int_{\Omega_F} q(\nabla\cdot\mathbf{u}+p/\kappa) d\Omega \quad (4.32)$$

$$(\mathbf{w},\mathbf{f})_{\Omega_F} = \int_{\Omega_F} \mathbf{w}\cdot\mathbf{f} d\Omega \quad (4.33)$$

$$(\mathbf{w},\mathbf{t})_{\partial\Omega_F^N} = \int_{\partial\Omega_F^N} \mathbf{w}\cdot\mathbf{t} d\Omega \quad (4.34)$$

$$e(\sigma_E,\mathbf{w})_{\Omega_E\cap\Omega_F} = \int_{\Omega_E\cap\Omega_F} \sigma_E : \nabla\mathbf{w} d\Omega \quad (4.35)$$

$$f(\sigma_E,\mathbf{w})_{\partial(\Omega_E\cap\Omega_F)} = \int_{\partial(\Omega_E\cap\Omega_F)} \mathbf{w}\cdot(\sigma_E\mathbf{n}) d\Omega \quad (4.36)$$

4.3.3 Galerkin formulation

The Galerkin finite element approximation of the weak form for the electrostatics problem can be stated as

find $\phi_{hp} \in X_{hp}$ such that

$$(\epsilon_r \nabla \phi_{hp}, \nabla w_{hp})_{\Omega_E} = \int_{\partial\Omega_E^N} \mathbf{n} \cdot \epsilon_r \nabla \phi_{hp} w_{hp} d\Omega + (\rho_V, w_{hp})_{\Omega_E} \quad \forall w_{hp} \in Y_{hp} \tag{4.37}$$

where $X_{hp} \subset X$ and $Y_{hp} \subset Y$. Likewise, the Galerkin counterpart for the weak form of the penalty function formulation is stated as

find $\mathbf{u}_{hp} \in \mathbf{V}_{hp}$ such that

$$\begin{aligned} a(\mathbf{u}_{hp}, \mathbf{w}_{hp})_{\Omega_F} = (\mathbf{u}_{hp}, \mathbf{f})_{\Omega_F} + (\mathbf{w}_{hp}, \mathbf{t})_{\partial\Omega_F^N} + b(\sigma_E(\phi_{hp}), \mathbf{w}_{hp})_{\Omega_E \cap \Omega_F} \\ + c(\sigma_E(\phi_{hp}), \mathbf{w}_{hp})_{\partial(\Omega_E \cap \Omega_F)} \end{aligned} \tag{4.38}$$

$\forall\ \mathbf{w}_{hp} \in \mathbf{W}_{hp}$. Similarly the Galerkin counterpart for the weak form of the mixed method is stated as

find $\mathbf{u}_{hp} \in \mathbf{V}_{hp}$ and $p_{hp-1} \in Z$ such that

$$\begin{aligned} d(\mathbf{u}_{hp}, \mathbf{w}_{hp})_{\Omega_F} - (\nabla \cdot \mathbf{w}_{hp}, p_{hp-1})_{\Omega_F} = (\mathbf{w}_{hp}, \mathbf{f})_{\Omega_F} + (\mathbf{w}_{hp}, \mathbf{t})_{\partial\Omega_F^N} \\ + e(\sigma_E(\phi_{hp}), \mathbf{w}_{hp})_{\Omega_E \cap \Omega_F} + f(\sigma_E(\phi_{hp}), \mathbf{w}_{hp})_{\partial(\Omega_E \cap \Omega_F)} \end{aligned} \tag{4.39}$$

and

$$-(q_{hp-1}, \nabla \cdot \mathbf{u}_{hp} + p_{hp-1}/\kappa)_{\Omega_F} = 0 \tag{4.40}$$

$\forall\ \mathbf{w}_{hp} \in \mathbf{W}_{hp}$ and $q_{hp-1} \in Z_{hp-1}$ where $\mathbf{V}_{hp} \subset \mathbf{V}$ and $\mathbf{W}_{hp} \subset \mathbf{W}$ and $Z_{hp-1} \subset Z$. Next the algorithm implemented in the project for the coupled solver is shown.

4.4 Coupled solver strategy

As was explained at the beginning of this chapter, the coupling of the electrostatics and fluid mechanical fields is due to the source term appearing in the governing equation of Stokes flow, which is due to the electrostrictive effects. The source term being $\nabla \cdot \sigma_E$. The electrostrictive stress σ_E is a function of the electric field, which, in turn, is a function of the electrostatic potentials. The form of the coupling in this

case is one-way since the computed velocities and pressure for the electrostrictive fluid does not affect the electrostatic field. In other words the permittivity in the electrostatic field is invariant to the velocity and pressure field. The algorithm which is implemented is shown below.

Algorithm 1 One-way coupling algorithm

▷ Input ϵ_r

▷ Compute ϕ_{hp} in the electrostatics field problem

▷ Compute $E = -\nabla\phi_{hp}$

▷ Set $\sigma_E = \epsilon_r \mathbf{E} \otimes \mathbf{E} - \frac{\epsilon_r}{2}(\mathbf{E} \cdot \mathbf{E})\mathbb{I}$

▷ Compute $\mathbf{u}_{hp}$ by solving eq. (4.38) or eq. (4.39)

4.5 Benchmark example

The benchmark example chosen for this problem is illustrated in Figure. 4.2, which is case of an infinite fluid domain with rigid dielectric insert subjected to unidirectional compression($\mathbf{t}$) and uniform Electric field ($\mathbf{E}$) in the infinity. Also in the same figure, the permittivity of the insert and the fluid domain are explicitly denoted. This benchmark example is very similar to the one shown in [21], where an infinite linear elastic plate is subjected to unidirectional tension. In [21], an analytical solution for the coupled solution of an electrostrictive plate under the assumption of one-way coupling between linear elasticity and electrostatics was derived. Based on the analogy shown in chapter 3 between Stokes flow and linear elasticity, one uses this analytical solution as an approximate analytical solution for the coupled problem of electrostrictive fluid in this domain by choosing $\nu \approx 0.5$.

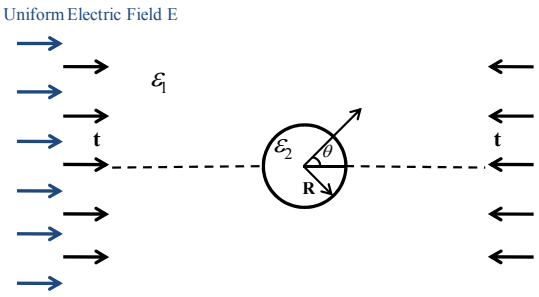

Figure 4.2: Benchmark problem for electrostriction

In order to simulate the coupled problem, a finite domain is chosen from the infinite domain. It is shown in Figure. 4.3. Initially the electrostatics problem is solved, where the exact solution of the electric potential ϕ is applied on the Dirichlet boundary. Subsequently for the electrostrictive fluid problem, the analytical tractions are applied on the Neumann boundary.

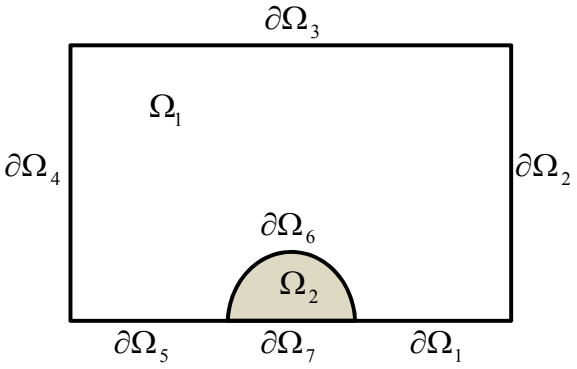

Figure 4.3: Finite domain for electrostriction benchmark problem

From the Figure. 4.3, the domains and boundaries of the electrostatics and the fluid problem are defined as follows. The domains and boundaries for electrostatics problem are given as

$$\begin{aligned} \Omega_E &= \Omega_1 \cap \Omega_2 \\ \partial\Omega_E &= \partial\Omega_1 \cup \partial\Omega_2 \cup \partial\Omega_3 \cup \partial\Omega_4 \cup \partial\Omega_5 \cup \partial\Omega_7 \end{aligned}$$

and subsequently the domains and boundaries for the fluid problem are given as

$$\begin{aligned} \Omega_F &= \Omega_1 \\ \partial\Omega_F &= \partial\Omega_1 \cup \partial\Omega_2 \cup \partial\Omega_3 \cup \partial\Omega_4 \cup \partial\Omega_5 \cup \partial\Omega_6 \end{aligned}$$

Next the input values for the benchmark problem is defined,

$$\begin{aligned} R &= 1 \\ \mathbf{E}_\infty &= 1 \\ \epsilon_r^f &= 2 \\ \epsilon_r^h &= 1 \end{aligned}$$

where R is the radius of the dielectric insert and where ϵ_r^f and ϵ_r^h are the permittivities of the fluid and the dielectric insert respectively. Furthermore, symmetry boundary conditions are applied along the symmetry plane and zero displacement conditions are applied at the interface of the fluid domain and the rigid insert. Moreover, the Poisson's ratio used in the simulation is $\nu = 0.4999$. Next, the numerical results for this benchmark problem will be shown after the next section.

4.6 Numerical exercise

In this section a novel coupled electrostrictive fluid problem is defined and corresponding numerical results are shown later. The benchmark problem for electrostatics, shown in chapter 1 and the lid driven cavity fluid problem, shown in chapter 3 are combined together to create this new coupled problem. The problem in the Figure. 4.4 will be solved.

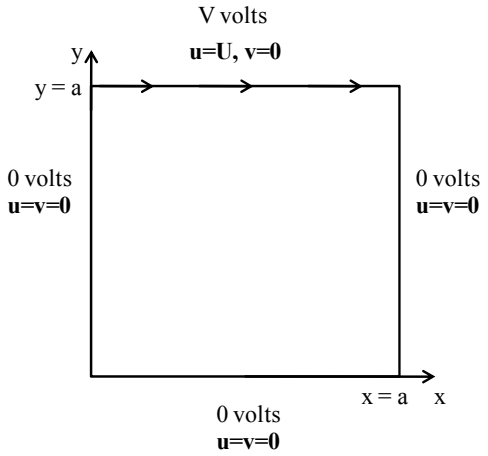

Figure 4.4: Domain and boundary conditions of the numerical example

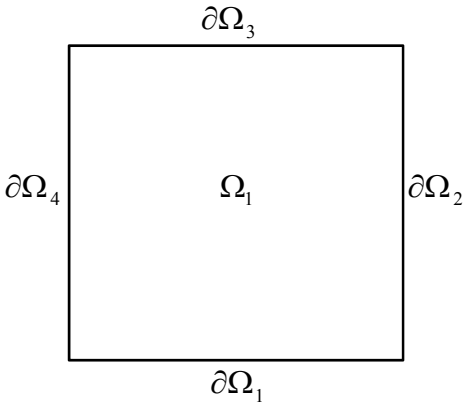

Figure 4.5: Finite domain for numerical exercise

From the Figure. 4.5, the domains and boundaries of numerical exercise are defined as follows. The domains and boundaries for electrostatics problem are given as

$$\begin{aligned} \Omega_E &= \Omega_1 \\ \partial\Omega_E &= \partial\Omega_1 \cup \partial\Omega_2 \cup \partial\Omega_3 \cup \partial\Omega_4 \end{aligned}$$

and subsequently the domains and boundaries for the fluid problem are given as

$$\begin{aligned} \Omega_F &= \Omega_1 \\ \partial\Omega_F &= \partial\Omega_1 \cup \partial\Omega_2 \cup \partial\Omega_3 \cup \partial\Omega_4 \end{aligned}$$

The findings of the simulation results of this problem will be shown in the next section.

4.7 Numerical results and discussion

First the numerical results for the benchmark problem is shown. The domain is discretized with unstructured mesh of triangular elements with uniform spacing $h = 0.4$ and order $p = 1,\ 2,\ 3,\ 4$ are applied. Furthermore, the geometry of the circular insert is represented exactly using the blending functions [10]. A typical mesh with spacing $h = 0.4$ is shown in Figure. 4.6.

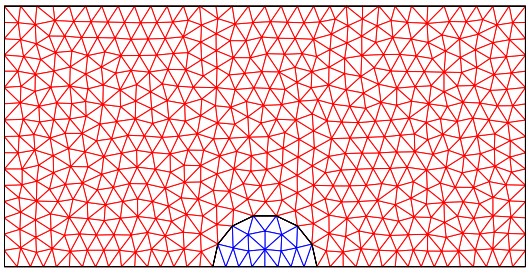

Figure 4.6: Mesh with uniform spacing of $h = 0.4$

The error is measured in the L^2 norm, the definitions of which are given in the appendix. The contour plot of the electric field for mixed method, with $h = 0.4$ and $p = 2$ is shown in Figure. 4.7. Also the velocities with the same order and spacing for mixed method is shown in Figure. 4.8.

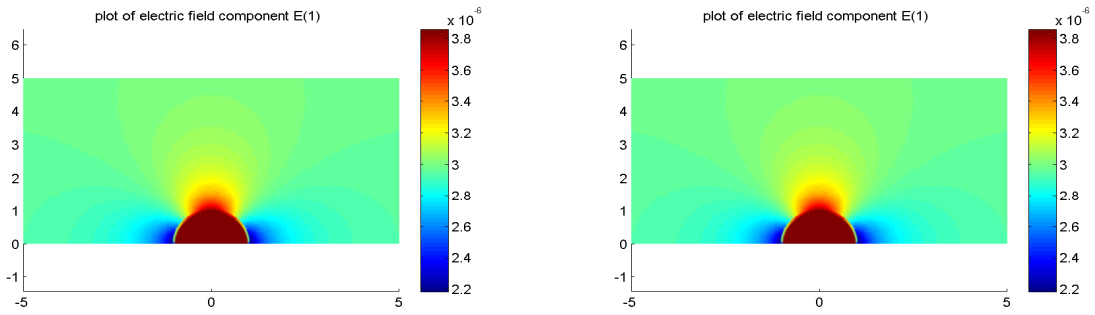

Figure 4.7: Contour plot of the electric field

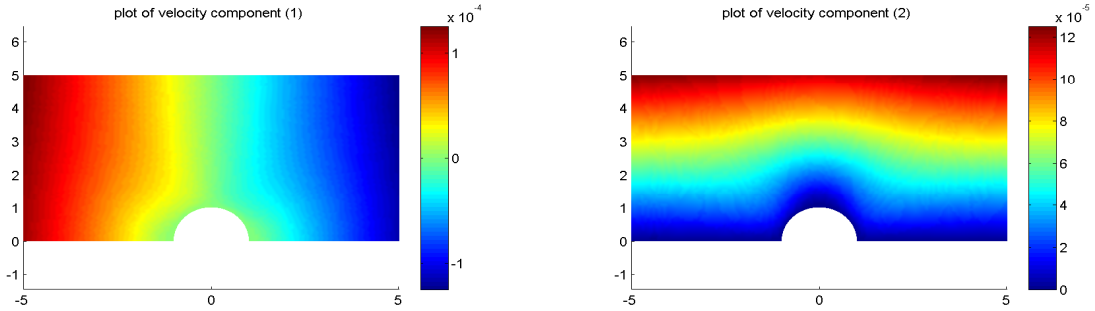

Figure 4.8: Contour plot of the velocity

The convergence plot for velocities is shown for the penalty function formulation and the mixed method in the Figure. 4.9. In both the cases a p refinement is done and the downwards sloping curve indicates exponential convergence of the solution. Here it is important to remark that, since penalty method and the mixed approach for the penalty formulation employ essentially the same methodology as the analytical solution (i.e. both are linear elastic solvers which act as regularized Stokes flow solvers), they converge exponentially fast to the analytical solution, which represents the exact solution of the linear elastic problem and not the Stokes flow solution.

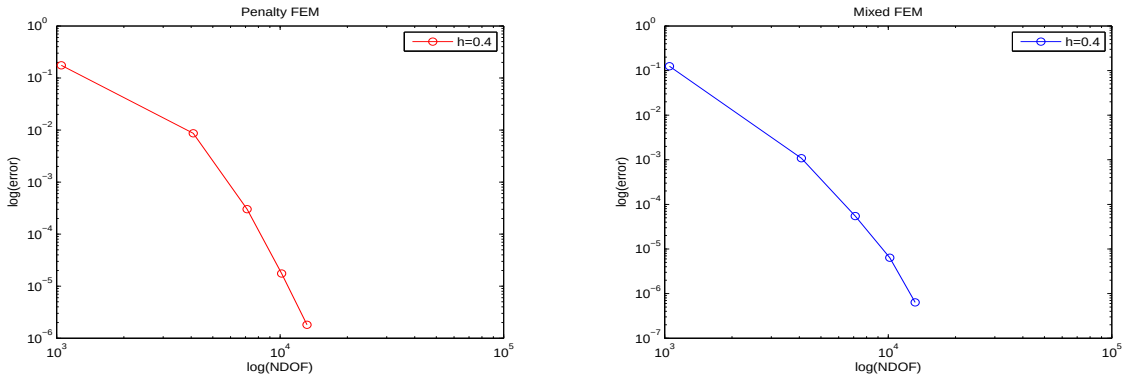

Figure 4.9: p convergence for the penalty and mixed methods

The error associated with using a regularized Stokes flow solution is not accounted for here, but, based on the solutions shown in chapter 3, it is believed to be small. Next the results for the numerical exercise of the cavity problem is shown. A mixed method is used for this simulation. A typical mesh with spacing $h = 0.1$ for this problem is shown in Figure. 4.10.

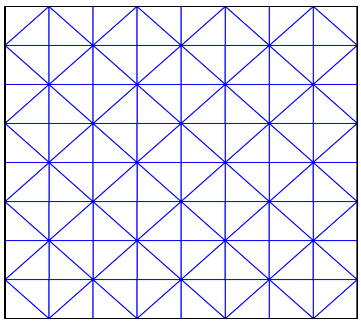

Figure 4.10: Mesh with uniform spacing of $h = 0.1$

The simulation is for order $p = 2$. Also the Poisson's ratio is 0.4999 and the viscosity of 0.3333. The vector plot of the velocity is obtained in order to get an intuitive picture of the flow pattern. These effects are shown in the Figure. 4.11.

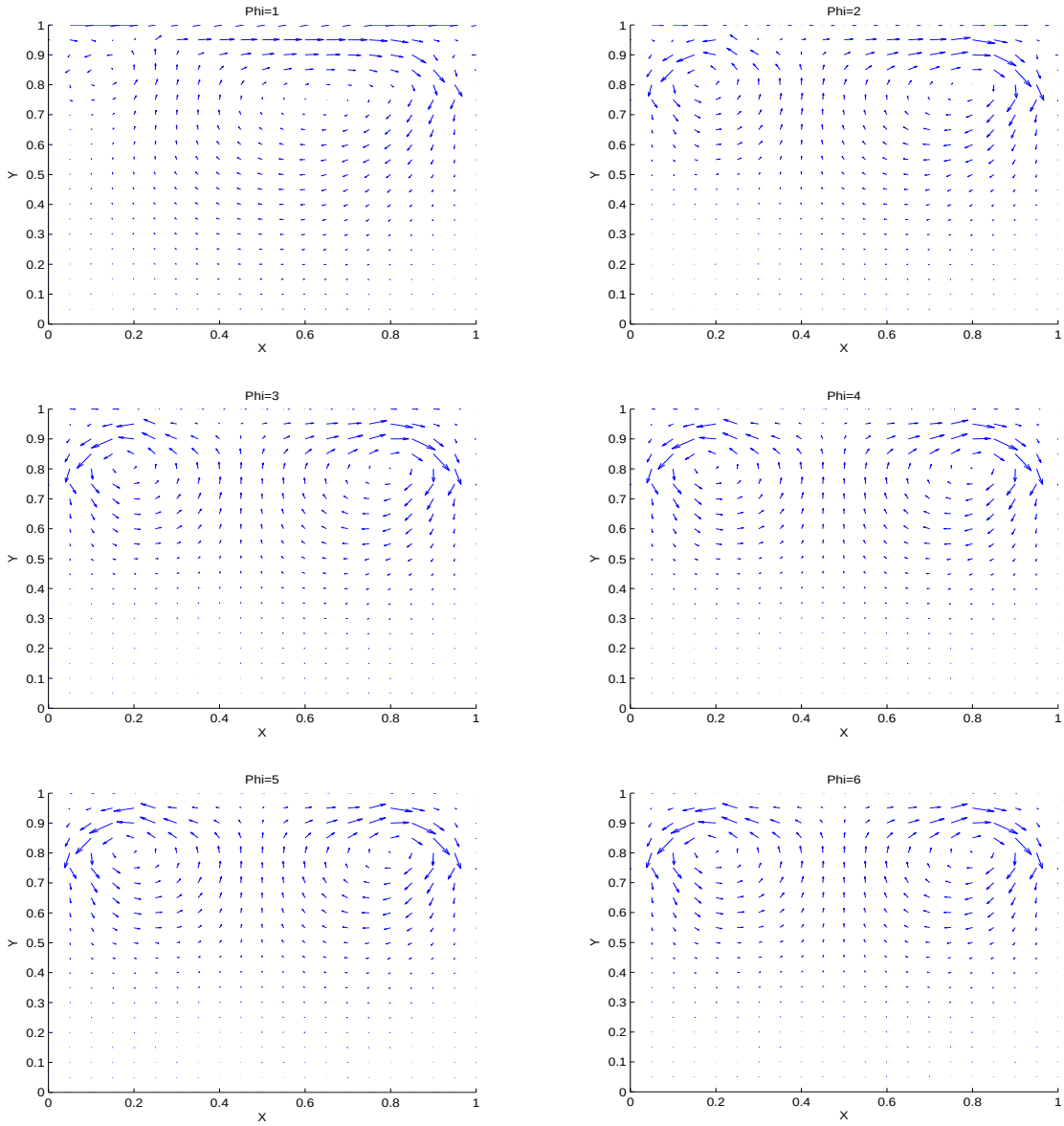

Figure 4.11: Velocity vector plots for various values of potentials ϕ

The sequence of results shown in Figure. 4.11, can be described as follows. The potential ϕ is applied on $\partial\Omega_3$. It is explained before how the value of applied potential affects the strength of the electric field and in turn, the electrostrictive stress. But excluding the effects of electrostriction, there is a flow circulation zone created at the center of the domain due to the applied velocity on the boundary $\partial\Omega_3$. However, when the electrostrictive effects are considered, the flow pattern changes. This change

begins when the value of ϕ changes. For small values of ϕ, the effects of the applied velocity is dominant. However, as the value of ϕ is increasing, the strength of the electric field grows, and so does the electrostrictive stress. Since this electrostrictive stress acts as a source term in the fluid problem, its dominance in the problem increases. This effect can be seen the Figure. 4.11. Due to the applied potentials, there is a counter vortex created and its strength increases as the value of ϕ increases.

Thus the finding from this simulation is that, for a constant velocity of the lid, when the applied potential is increased, there is a counter vortex generated at the top left corner.

The application of this numerical exercise may be used for simulation of electro-osmotic flow over a super-hydrophobic surface, which is a current research topic at Technical University of Darmstadt [1], where the coupling is very simular to the one described in the project. There are variety of applications for electro-osmotic flows, as described in chapter 1. Furthermore, there can be many type of extensions for this project, which are told in the next chapter.

Chapter 5

Conclusions

5.1 Conclusion

The objective of this project were to investigate and numerically analyze the coupled phenomena of electrostatics and fluid mechanics. The project was split into three parts, first the analysis of the electrostatics field, next the analysis of the fluid field, and then the coupled analysis of the electrostrictive fluid.

Initially the benchmark simulations for the electrostatics problem were performed. The benchmark problem contained two singularities at the top corners due to intersection between Dirichlet boundaries. The convergence for the problem was obtained using the analytical solution. The h, p and the hp refinements were utilized to obtain the convergence plots. It was found that the convergence for h refinement was algebraic as expected and for p refinement the convergence was exponential but the drop in the error was similar to the drop during h refinement. This was due to the singularities present in the problem. However, a non uniform mesh was utilized and hp refinement was done. It turned out that the convergence was faster and the error dropped more rapidly.

The fluid problem was simulated using the penalty function formulation and the mixed method for the penalty formulation (hence forth referred to as mixed method). Firstly, the penalty function formulation was used, where the solution is obtained only for the velocities and then the mixed method was used where the solution is obtained for both velocities and the pressure. Three different benchmark simulations were performed for both formulation for the same. Initially the Poiseiulle's flow problem

was solved, then the problem with a source term, and later the lid driven cavity problem was simulated. Exponential convergence was obtained for Poiseiulle's flow and the problem with a source term. The lid driven cavity problem was compared with the standard literature and the results were practically identical.

After performing the individual analysis of the electrostatics and the fluid field, the coupled problem is investigated. The key coupling phenomena arises due to the stresses created due to the electric field, which then acts as a source term in the fluid problem. The one-way coupling algorithm was implemented and the numerical results were benchmarked with an analytical solution. Moreover, exponential convergence was obtained using the p refinements. Furthermore, a novel numerical exercise is analyzed, so as to find how the coupling affects the flow physics of this particular problem. Possible applications include the electroosmotic flow, which is described in chapter 1.

Thus the objectives of this project are met to a satisfactory level, since all the results were benchmarked with the analytical solution and the available literature. A summary of the findings in this thesis work are listed as follows

1 Initial benchmarking simulations for the electrostatics problem was done with h, p and hp refinements and it is found that an optimal combination of h and p refinements result in exponential convergence for the problem with singularities.

2 During the simulation of the fluid field, it was found that the penalty function formulation exhibited locking behavior, which was then alleviated using successive p refinements.

3 It was found that the mixed method had much better conditioning of the stiffness matrix compared to the penalty function formulation, by observing the eigenspectrum of the element stiffness matrix.

4 The Poisson's ratio vs the error is plotted for the fluid problem and after successive increase in the Poisson's ratio the error decreased until a certain point, after

which the error increased. Thus an optimal value of the Poisson's ratio was obtained from this exercise.

4 The p convergence for the velocities in the benchmark problems of the fluid field with analytical solutions was exponential in nature.

5 Furthermore, the velocity profile obtained from the simulation of the lid driven cavity problem matched exactly with the one obtained in the standard literature. This further reiterates that the given code is benchmarked.

6 Next, the coupled solver was implemented and the results obtained for p refinements were exponential in nature.

7 The numerical exercise was simulated and it was found that as the magnitude of the applied potential is increased, its effect is more dominating in the flow, which is seen as the counter vortex created in the flow domain. This effect is because of the dominant source term in the fluid field, which is a function of the electric field.

5.1.1 Further work

As it is, the work in the thesis can be applied directly to the current research in the electroosmotic flows for the superhydrophobic surfaces [1]. Moreover, the chaotic mixing in microchannels using the electroosmotic flow can be simulated using the idea in the thesis. Possible immediate extensions will be to simulate such flows in 2D. Further extension could include the extension to 3 dimensional simulations and including unsteady effects, however, this could involve time integration and mass matrices which increases the complexity of the simulation. The simulation of electrostatic fluid accelerators also require the evaluation of current density, thus necessitating the solution of an additional PDE.

Other possible future extensions of the thesis could involve coupling the complete electromagnetic field and the fluid field, thus requiring the solution of the complete

set of Maxwell's equations and the full set of Navier-Stokes equations. This coupling phenomena is the magnetohydrodynamic phenomena. The applications of which, includes simulation of the Tokamak type nuclear reactors [22], simulation of solar winds [23], simulation of the earth's crust [24] etc.

Appendix A

Function Space Definitions and Error Norm

For a domain $\Omega \subset \mathbb{R}^d$, $d = 1, 2, 3$, one can define the function space $L_2(\Omega)$ of square integrable functions on Ω by saying that $f \in L_2(\Omega)$ if and only if

$$\|f\| := \left(\int_\Omega |f(x)|^2 dx \right)^{1/2} \quad < \infty \tag{A.1}$$

The norm f has the following properties

$$\begin{aligned} \|f\| &= 0 && \text{if and only if } f = 0 \\ \|f + g\| &= \|f\| + \|g\| && \text{for all } f, g \in L_2(\Omega) \\ \|\alpha f\| &= \alpha \|f\| && \text{for all } \alpha \in \mathbb{R}, f \in L_2(\Omega) \end{aligned} \tag{A.2}$$

Also the Sobolev space $H^1(\Omega)$ is defined by saying that $f \in H^1(\Omega)$ if and only if

$$\|\nabla f\|^2 + \|f\|^2 < \infty \tag{A.3}$$

which implies both the function and its gradient must be square integrable. Furthermore, the L_2 norm of the error, which is used for showing the convergence plots in various chapters, is defined as

$$\|e\|_{L_2} = [\int_\Omega (u_{exact} - u_{FE})^2 d\Omega]^{1/2} \tag{A.4}$$

where u_{exact} represents the exact solution and u_{FE} is the finite element solution.

Appendix B

Numerical Results for Helmholtz Equation in 1D

In the first chapter, there was a discussion on higher order shape functions in one dimension. These shape functions are used for the finite element solution of the Helmholtz problem in one dimension. The problem is initially defined and the results are discussed later.

B.1 Problem Description

Many problems related to wave propagation are governed by Helmholtz equation. Here only 1D Helmholtz equation is analysed since the main purpose of this chapter is to understand why higher order approximations are used. The strong form of the Helmholtz equation with the given set of boundary conditions, is defined as

$$\nabla^2\phi + k^2\phi = 0 \text{ in } \Omega \tag{B.1}$$

$$\phi(x_0) = \phi_0 \tag{B.2}$$

$$\phi(x_L) = \phi_L \tag{B.3}$$

where k is the wave number which is taken as a constant. In this problem only one dimension analysis is done. The corresponding domain for the problem can be visualized in the Figure B.1.

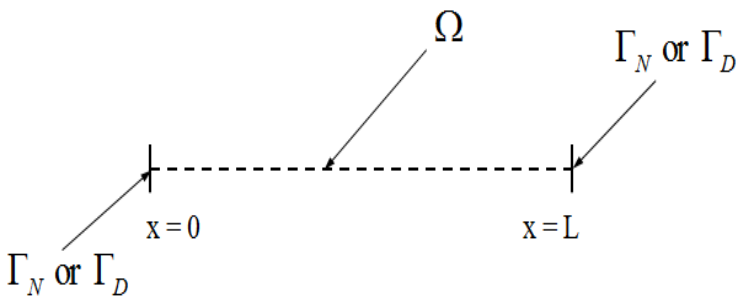

Figure B.1: Domain and possible boundary condition for the given electrostatics problem

where $\Omega = 0 \leq x \leq L$ is the problem domain, Γ_N is the Neumann boundary condition and Γ_D is the Dirichlet boundary condition. It is an one dimensional problem. In this particular case analyzed, the boundary condition on both ends of the domain is given to be Dirichlet type. The analytical solution of the Helmholtz Boundary Value Problem (BVP) with the given set of boundary conditions simplifies to be

$$\phi = A\cos px + B\sin px \tag{B.4}$$

and the boundary conditions are

$$\phi(x_0) = \phi_0 \quad and \quad \phi(x_L) = \phi_L \tag{B.5}$$

so the values of A and B are

$$A = \phi_0 \quad and \quad B = (\phi(x_L) - \phi_0 coskL)/(sinkL) \tag{B.6}$$

B.2 Finite element solution

Before solving in a computer it is needed to get the weak form of the problem. And from the weak form the linear system to be solved is obtained. After that the discretization is performed and then the employment of the higher order shape functions are discussed.

B.2.1 Derivation of the weak form and the formulation

Considering a general case i.e. equation defined is common in all three spatial dimensions. Now a weighting function w is used and the Helmholtz equation is integrated over the domain Ω

$$\int_{\Omega}(\nabla^2\phi + k^2\phi)wd\Omega = 0 \tag{B.7}$$

$$\int_{\Omega} w\nabla^2\phi d\Omega = -\int_{\Omega} k^2\phi w d\Omega \tag{B.8}$$

but in order to integrate by parts chain rule is used, $w\nabla^2\phi = w\nabla\cdot\nabla\phi = \nabla\cdot(w\nabla\phi) - \nabla w\cdot\nabla\phi$. Therefore,

$$\int_{\Omega}(\nabla\cdot(w\nabla\phi) - \nabla w\cdot\nabla\phi)d\Omega = -\int_{\Omega} k^2\phi w d\Omega \tag{B.9}$$

$$\int_{\Omega}\nabla\cdot(w\nabla\phi)d\Omega - \int_{\Omega}\nabla w\cdot\nabla\phi d\Omega = -\int_{\Omega} k^2\phi w d\Omega \tag{B.10}$$

Now using the divergence theorem implies $\int_{\Omega}\nabla\cdot(w\nabla\phi)d\Omega = \int_{\partial\Omega}\mathbf{n}\cdot(w\nabla\phi)dS$ Therefore Eq.(B.10) becomes

$$\int_{\Omega}\nabla w\cdot\nabla\phi d\Omega - \int_{\Omega} k^2\phi w d\Omega = \int_{\partial\Omega}\mathbf{n}\cdot(w\nabla\phi)dS \tag{B.11}$$

So the problem presents itself as to find $\phi \in H^1(\Omega)$ such that

$$\int_{\Omega}\nabla w\cdot\nabla\phi d\Omega - \int_{\Omega} k^2\phi w d\Omega = \int_{\partial\Omega}\mathbf{n}\cdot(w\nabla\phi)dS \quad \forall w \in H^1(\Omega) \tag{B.12}$$

The above equation is known as the weak form of the problem, where $H^1(\Omega)$ is called the Sobolev space. Now, for the one dimensional case considered here, the succeeding equations can be alternatively written as

$$\left[w\frac{d\phi}{dx}\right]_0^L - \int_0^L \frac{\partial\phi}{dx}\frac{dw}{dx}dx + \int_0^L k^2\phi w dx = 0 \tag{B.13}$$

Following the finite element method ϕ is expanded as

$$\phi \approx \phi_H = \sum_{i=1}^{M}\phi_i N_i(x,y) \tag{B.14}$$

It is known that by Galerkin's method the weighting functions are chosen as the shape functions themselves [15] i.e. $N_i(x,y)$ $(i = 1, 2, ...m)$.

Therefore from Eq. B.13 becomes

$$\int_0^L \frac{dN_i}{dx}\frac{dN_j}{dx}dx - \int_0^L k^2 N_i N_j dx = \left[N_i \frac{d\phi}{dx}\right]_0^L \tag{B.15}$$

which further reduces to

$$[K - k^2 M]\phi = b \tag{B.16}$$

where K is the stiffness matrix, M is the mass matrix and b is the load vector, given as

$$K = \int_0^L \frac{dN_i}{dx}\frac{dN_j}{dx}dx,\ M = \int_0^L k^2 N_i N_j dx \ and\ b = \left[N_i \frac{d\phi}{dx}\right]_0^L \tag{B.17}$$

B.3 Higher order shape functions

This section describes the higher order shape functions used in the finite element analysis. Their utility and advantages are already explained in chapter 1. The higher order shape functions are of two basic types. One is the nodal type and the other is the hierarchical type. In the nodal approach the degrees of freedom correspond to specific solution points. For the one dimensional problem discussed, the nodal shape functions are shown in chapter 1. Regarding the hierarchical shape function, there are three versions. The version 1 is shown in [11]. The version 2 is an improvement over version 1 since these shape functions can extend to higher orders than cubic approximations. They are defined as

$$N_p(\xi) = \begin{cases} \frac{1}{p!}(\xi^p - 1) \\ \frac{1}{p!}(\xi^p - \xi) \end{cases}, \quad \frac{dN_p}{d\xi} \begin{cases} \frac{1}{p!}(p\xi^{p-1}) \\ \frac{1}{p!}(p\xi^{p-1} - 1) \end{cases} \tag{B.18}$$

where p$\geq$ 2 is the order of the polynomial. Next the version 3 of the hierarchical shape function is defined as the integral of each set of polynomials from $-1 \leq \xi \leq 1$. This polynomial is called as Legendre polynomial. It is defined as

$$P_p(\xi) = \frac{1}{(p-1)!}\frac{1}{2^{p-1}}\frac{dP^p}{d\xi^p}[(\xi^2 - 1)^p] \tag{B.19}$$

The corresponding shape functions are

$$N_p(\xi) = \frac{1}{2p-1}\big(P_p(\xi) - P_{p-2}(\xi)\big),\ \frac{dN_p}{d\xi}(\xi) = \frac{1}{2p-1}\left(\frac{dP_p}{d\xi}(\xi) - \frac{dP_{p-1}}{d\xi}(\xi)\right) \quad \text{(B.20)}$$

More on these shape functions are given in [11].

B.4 Results and discussion

The computer program in [11] is utilized to obtain the results. Furthermore MATLAB scripts are written to obtain the convergence plots for the results. These plots are for a particular wave number of 20 unless otherwise stated, and for uniform mesh discretization. The euclidean norm is used to calculate the error between the numerical and the exact solution. The absolute and relative error are shown as follows

$$e_{abs} = |\phi_{exact} - \phi_{numerical}|^2 \quad \text{and} \quad e_{rel} = |\phi_{exact} - \phi_{numerical}|^2/\phi^2_{exact} \quad \text{(B.21)}$$

and the Euclidean norm $||\overrightarrow{e}|| = \sqrt{\sum_{i=1}^{n} |\overrightarrow{e}|^2}$. The plots shown in the following gives a strong indication as to why the higher order method and subsequently why the hierarchical forms of the shape functions are being utilized. The following is the discussion for the version one of the shape functions employed. First the nodal and hierarchical shape functions are compared for h and p refinement. Comparing Figure B.2 and Figure B.3 it is observed that they have almost similar convergence trend for h refinement. However, while comparing them for p refinement shows that the convergence is exponential as it is shown in Figure B.4.

Furthermore the Figure B.4 shows the plots for nodal shape functions. Figure B.5 shows the convergence with hierarchical shape functions. The convergence is again exponential. Thus is can be ascertained that convergence is better in the case of p refinement compared to h refinement.

Next we compare the nodal and hierarchical shape functions which are used, with respect to the condition number. The logarithm of condition number is in the y axis

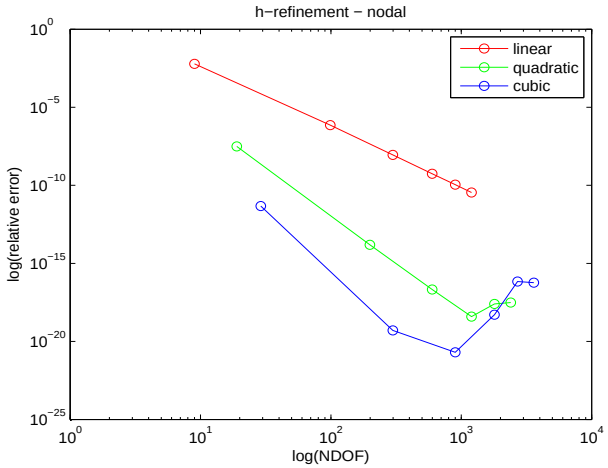

Figure B.2: h refinement with nodal shape functions

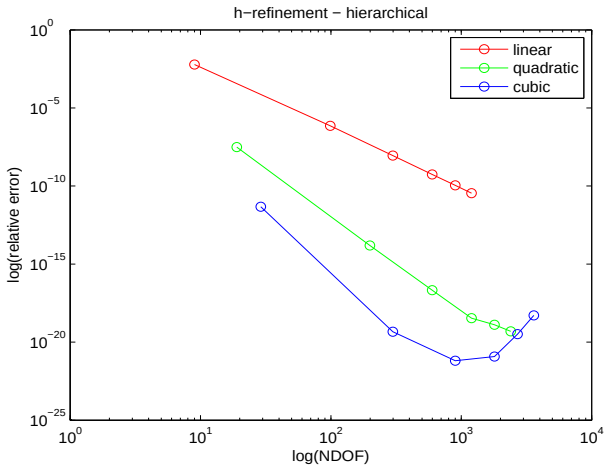

Figure B.3: h refinement with hierarchical shape functions

and the order p is in the x axis. In the Figure B.6 the condition number versus the order is shown.

It is clear that hierarchical shape function proves to be having better conditioning properties for the stiffness matrix than the nodal shape function. However the above discussion was for version one of the shape functions which were discussed before. Current implementation of the version one has a limitation that it cannot be used for orders greater than three, but the versions two and three are capable of going

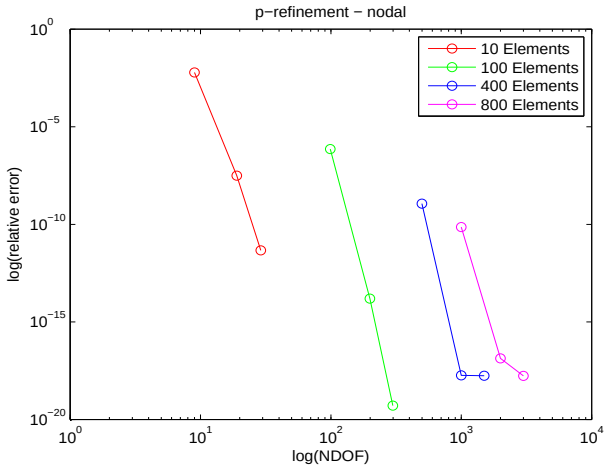

Figure B.4: p refinement with nodal shape functions

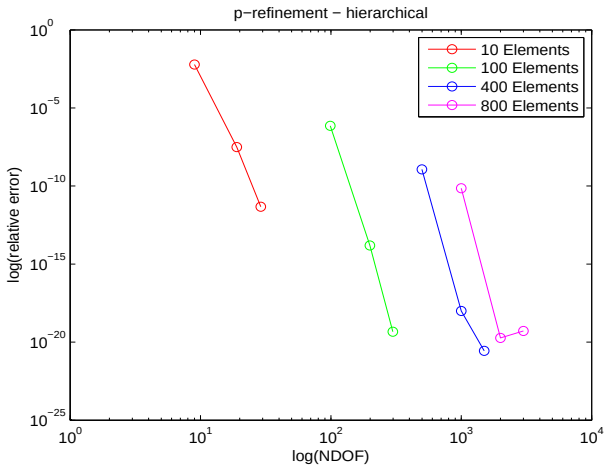

Figure B.5: p refinement with hierarchical shape functions

beyond order three. Now the results for version two and version three of the shape functions are discussed and compared with each other. Figure B.7 and Figure B.8 shows the h refinement for a quadratic order. It is observed that the convergence is linear.

Next results for p refinement is shown for versions two and three in Figure B.9 and Figure B.10. It is seen that the convergence is exponential. It can be inferred that p refinement is again better than h refinement for Helmholtz problem, and for

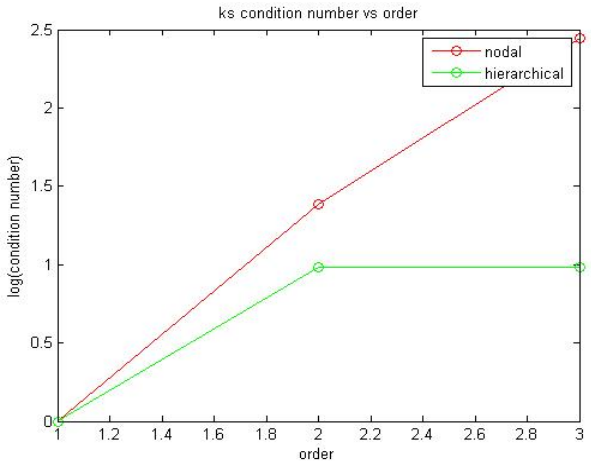

Figure B.6: Condition number comparison of the stiffness matrix for nodal and hierarchical approach

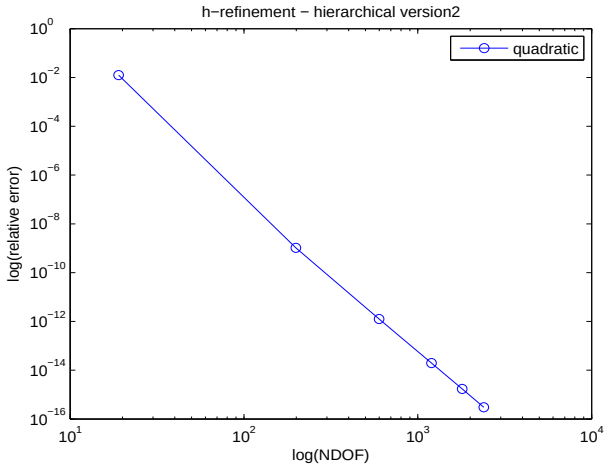

Figure B.7: h refinement for hierarchical shape functions - version 2

similar problems with no singularities. The versions two and three show in depth convergence compared to version one.

Next the condition number for the stiffness matrix is compared for all the versions in the Figure B.11. The wave number used was $k = 1$, since for higher wave numbers the numerical solution has decreasing accuracy, the phenomenon called pollution. This effect is due to the reason that the wave number of the exact solution is different

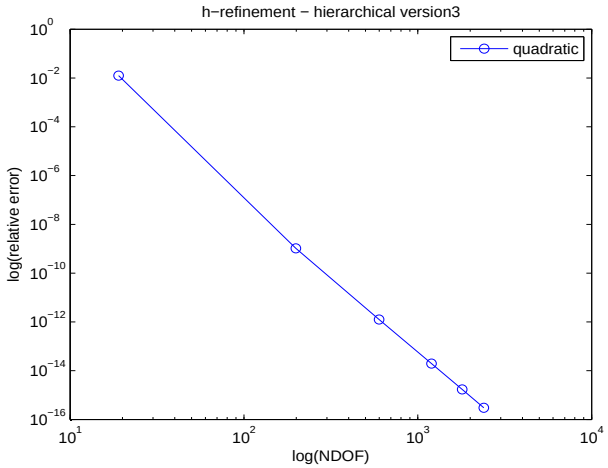

Figure B.8: h refinement for hierarchical shape functions - version 3

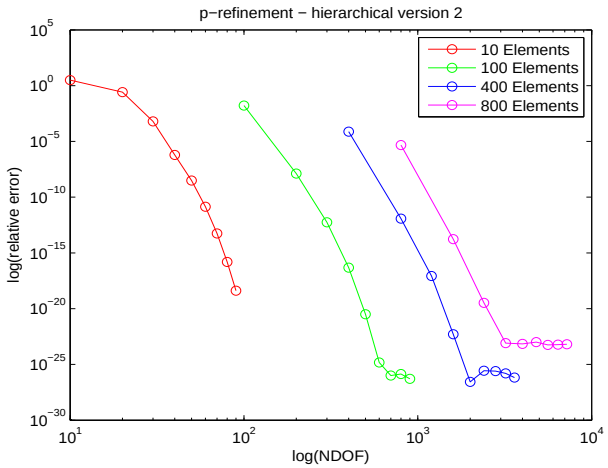

Figure B.9: p refinement for hierarchical shape functions - version 2

from the numerical one, the effect being called dispersion [11]. More on dispersion and pollution effects can be found in [25] and will not be discussed presently since it is beyond the scope of the thesis.

It can be noted that the version three is the best one among the others since the condition number increases very slowly with increase in order as compared to the versions one and two. Since conditioning of the stiffness matrix determines its stability, the version three can be chosen as the best option for numerical implementation

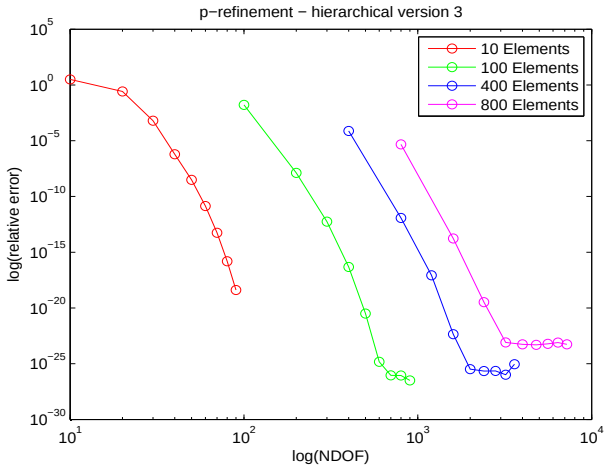

Figure B.10: p refinement for hierarchical shape functions - version 3

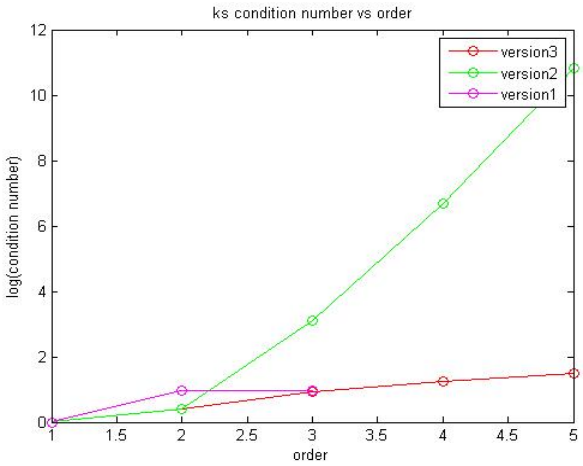

Figure B.11: Condition number comparison of the stiffness matrix for different versions of the hierarchical shape shape functions

of such problems. Apart from the discussion on comparison of the shape functions used here, the main point to be emphasized is that the p refinement results in exponential convergence always with exception to the presence of singularities. So even though the higher order shape functions prove to be difficult implementation wise, they are definitely superior to that of the h refinement. Other conclusion is that the hierarchical shape functions are proving to be better than the nodal shape functions

in terms of implementation as well as the conditioning of the stiffness matrix. Thus the above conclusions about the results of the Helmholtz problem coincide with the initial discussion on higher order shape functions in chapter 1.

Bibliography

[1] C. Steffes. Modeling of flow over superhydrophobic surfaces under the influence of electric fields, June 2008.

[2] J. Donea and A. Huerta. *Finite Element Methods for Flow Problems*. Wiley, 2004.

[3] U. Ghia K.T. Ghia and C.T. Shin. High-re solutions for incompressible flow using the navier-stokes equations and the multigrid method. *Journal of Computational Physics*, 48:387–411, 1982.

[4] J.N. Reddy and D.K. Gartling. *The Finite Element Method in Heat Transfer and Fluid Mechanics*. CRC Press, 1994.

[5] S. Yakota. Micro actuators using functional fluids. *The Fourth International Symposium on Fluid Power Transmission and Control*, 2003.

[6] I. Genuth. Ionic wind - chillin' the pc, January 2007.

[7] J.R. Pacheco et.al. Enhancement of chaotic mixing in electroosmotic flows by random period modulation. *Proceedings of IMECE2007 2007 ASME International Mechanical Engineering Congress and Exposition*, 2007.

[8] O.C. Zienkiewicz and R.L. Taylor. *Finite Element Method: Volume 1*. Butterworth-Heinemann, 2000.

[9] O.C. Zienkiewicz and K. Morgan. *Finite Elements and Approximation*. Wiley, 1983.

[10] B. Szabo and I. Babuska. *Finite Element Analysis*. Wiley, 1991.

[11] N. Hamlyn. *Level 3 Research Project*. Swansea UK, 2010.

[12] J.C. Maxwell. *A treatise on Electricity and Magnetism, vol. I.* Dover, 1954.

[13] J.C. Maxwell. *A treatise on Electricity and Magnetism, vol. II.* Dover, 1954.

[14] P.D. Ledger. *Notes on Computational Electromagnetics, Swansea University.* Swansea UK, 2010.

[15] T.J.R. Hughes. *Linear Static and Dynamic Finite Element Analysis.* Dover, 2000.

[16] J. Schoberl and S. Zaglmayr. Higher order nedelec elements with local complete sequence properties. *International Journal for Computation and Mathematics in Electrical and Electronic Engineering (COMPEL)*, 24:374–384, 2005.

[17] Lan Jin. *Finite Element Analysis of Coupled Electrostrictive Materials.* Swansea UK, 2010.

[18] W.K. Liu T.J.R. Hughes and A. Brookes. Finite element analysis of incompressible viscous flows by the penalty function method. *Journal of Computational Physics*, 30:1–60, 1979.

[19] J. Bonet and R. D. Wood. *Nonlinear Continuum Mechanics for Finite Element Analysis.* Cambridge University Press, 1997.

[20] A.J. Gil. *Notes on Coupled Electrostrictive Materials, Swansea University.* Swansea UK, 2010.

[21] A.J. Gil and P.D. Ledger. A coupled *hp*-finite element scheme for two-dimensional electrostriction. *International Journal for Numerical Methods in Engineering*, Submitted.

[22] R. Paccagnella et al. 3d mhd vde and disruptions simulations of tokamaks plasmas including some iter scenarios. *Nuclear Fusion*, 2009.

[23] Raeder et al. *Geomagnetic Storm Simulation With a Coupled MagnetosphereIonosphereThermosphere Model*. UCLA California, 1997.

[24] Fearn. Magnetostrophic magnetoconvection. *Physics of Earth and Planetary Interiors*, 2000.

[25] A. Daraemaeker and I. Babuska. Dispersion and pollution of the fem solution for the helmholtz equation in one, two and three dimensions. *International Journal for Numerical Methods in Engineering*, 46:471–499, 1999.